

Higher-dimensional magnetic Skyrmions

Sven Bjarke Gudnason,^{1,*} Stefano Bolognesi,^{2,†} Roberto Menta^{3,‡}

¹Institute of Contemporary Mathematics, School of Mathematics and Statistics,
Henan University, Kaifeng, Henan 475004, P. R. China

²Department of Physics “E. Fermi”, University of Pisa, and INFN, Sezione di Pisa
Largo Pontecorvo, 3, Ed. C, 56127 Pisa, Italy

³Scuola Normale Superiore, Piazza dei Cavalieri, 7, and Laboratorio NEST,
Piazza S. Silvestro, 12, 56127 Pisa, Italy

November 20, 2024

Abstract

We propose a generalization of the theory of magnetic Skyrmions in chiral magnets in two dimensions to a higher-dimensional theory with magnetic Skyrmions in three dimensions and an S^3 target space, requiring a 4-dimensional magnetization vector. A physical realization of our theory necessitates the use of a synthetic dimension, recently promoted and realized in condensed matter physics. In the simplest incarnation of the theory, we find a Skyrmion and a sphaleron – the latter being an unstable soliton. Including also the Skyrme term in theory enriches the spectrum to a small metastable Skyrmion, an unstable sphaleron and a large stable Skyrmion.

*gudnason@henu.edu.cn

†stefano.bolognesi@unipi.it

‡roberto.menta@sns.it

Contents

1	Introduction	2
2	Higher-dimensional magnetic Skyrmions	4
2.1	Generalized DM Interaction	5
2.1.1	Bloch-type DMI	5
2.1.2	Néel-type DMI	9
2.1.3	Axially symmetric DMI	10
2.2	Spherically symmetric magnetic Skyrmions	11
2.2.1	Full equations of motion	13
2.2.2	Numerical Skyrmion solutions	14
2.2.3	Restricted model	16
2.2.4	The anti-Skyrmion	18
2.3	Magnetic sphalerons	19
2.3.1	Numerical sphaleron solutions	20
2.4	A connection to the Hopfion	23
3	A magnetic-QCD hybrid Skyrme model	25
3.1	Derrick phase diagram	26
3.2	Numerical magnetic-QCD hybrid Skyrmion solutions	28
3.3	Connecting to the Hopfion	31
4	Physical realization of higher-dimensional magnetic solitons	32
5	Conclusion	35

1 Introduction

The magnetic Skyrmion is gaining recognition as a prominent soliton in 2-dimensional magnetic physics, particularly in the context of chiral magnets and thin films [1–5], as well as spintronics and quantum technologies [6–9]. The name Skyrmion comes from the 3-dimensional soliton in the Skyrme model, proposed by T. Skyrme in the 1960s as a model of the nucleus [10, 11], further validated as a low-energy effective field theory of QCD at large N_c (number of colors) by E. Witten [12, 13] and later used as a validation of the Sakai-Sugimoto model as evidence that the model really describes QCD at low energies [14]. The Skyrmion in 2 or 3 dimensions is a texture soliton, which differs from a defect-type soliton by mapping the entire 2- or 3-dimensional space to the target space. In

particular, a magnetic Skyrmion in two dimensions is mapping the entire plane to an S^2 target space, with the latter being the normalized magnetization vector $\mathbf{n} = (n^1, n^2, n^3)$ such that $\mathbf{n} \cdot \mathbf{n} = 1$ [15–28]. It differs drastically from the 3-dimensional Skyrmion by the fact that: 1) it is stabilized by a *lower*-dimensional operator (i.e. less derivatives than number of spatial dimensions) and 2) it is chiral. The latter implies that magnetic Skyrmions stably exist, but no anti-Skyrmions exist. This is different from 3-dimensional Skyrmions, where a higher-dimensional operator (i.e. more derivatives than number of spatial dimensions) is used to stabilize the soliton – called a Skyrmion – against collapse. Indeed the higher-derivative (or smaller-derivative) terms are a way to avoid Derrick’s theorem [29].

In this paper, we consider the generalization of the 2-dimensional magnetic Skyrmion with target space S^2 to a 3-dimensional magnetic Skyrmion with target space S^3 .¹ Since the unit magnetization vector in three dimensions gives rise to S^2 , we need a unit magnetization vector in *four* dimensions.² We will henceforth denote the construct as a higher-dimensional magnetic Skyrmion.

The physical realization of a 3-dimensional magnetic Skyrmion would necessitate the incorporation of a synthetic (extra) dimension, as has been demonstrated in a number of physical systems – e.g. see Refs. [31–40]. Until now, the 3-dimensional counterpart of 2D magnetic Skyrmions were magnetic Hopfions, 3-dimensional solitons living in a magnetization vector that is also living in three dimensions. Recent numerical computations [41–45] suggest that similar objects may exist at the nanoscale in frustrated and chiral magnets. Micrometer-sized Hopfions have recently been created and observed experimentally in chiral ferromagnetic fluids [46, 47]. The 3D magnetic Skyrmions which we propose, instead, have S^3 as a target space, the same as used in the standard Skyrme model in three dimensions.

In this paper, we concentrate on the spherically symmetric case which enjoys $SO(3)$ invariance. We take the generalized Dzyaloshinskii-Moriya interaction (DMI) [48–50] to have only one derivative of the magnetization vector and a single component of the same vector. In four dimensions, this means that such a term must be contracted with a tensor that possesses two $SO(4)$ -indices and a single spatial index: we denote such a tensor by Θ . $SO(4)$ invariance dictates that Θ is antisymmetric in $SO(4)$ -indices and we use this fact, as well as global rotations to rotate the tensor to its *standard form*. We further impose $SO(3)$ invariance, where we are locking spatial rotations with an $SO(3) \subset SO(4)$ rotation, in order to obtain a spherically symmetric soliton. This procedure leads to *two* different

¹A preliminary investigation started in [30].

²We use the notation “magnetization vector” for the 4-dimensional generalization of the 3-dimension magnetization vector, although it is physically different. For example, it is not possible to write $\mathbf{B} \cdot \mathbf{n}$, since the 3-dimensional magnetic field has 3 components and a would-be 4-dimensional magnetic field cannot be dualized to a vector (the 4-dimensional Hodge dual of a 2-form is also a 2-form).

invariant structures in the Θ tensor. However, only one of these two structures remains nonvanishing when a spherically symmetric Ansatz is imposed. We furthermore show that both the Bloch-type and the Néel-type DMI generalizations lead to the same term when $\text{SO}(3)$ invariance is imposed.

A special feature of this higher-dimensional magnetic Skyrme model, is that it has multiple solutions. Indeed in its simplest incarnation, it has a Skyrmion and a sphaleron [51], with the latter being unstable and much smaller than the Skyrmion. Finally, we further extend the model by including the standard S^3 Skyrme term, which further enriches the phase diagram of the model, by engendering the model with a small metastable Skyrmion, an unstable sphaleron and a stable Skyrmion – at least in a finite region of the model’s parameter space.

The paper is organized as follows. In Sec. 2, we consider the minimal generalization of 2D magnetic Skyrmions to 3D magnetic Skyrmions with a 4-dimensional magnetization vector. In particular, in Sec. 2.1 we consider the generalizations of the DM term and its reductions due to symmetry considerations. In Sec. 2.2, we then study spherically symmetric Skyrmions numerically and consider the limit of the kinetic term being absent, leading to the so-called restricted model (analogous to other Skyrme-type models). In Sec. 2.3, we then turn to unstable solitons – the sphalerons of the theory – which are the smaller ones and harder to find. In Sec. 2.4, we describe a limit with an additional potential, in which the model eventually reduces to a chiral magnetic Hopfion model. In Sec. 3, we then consider including the Skyrme term which enriches the theory with an extra and tiny Skyrmion that is only metastable. In Sec. 4, we discuss the possibility of using a synthetic dimension to realize our theory in the real world. We conclude in Sec. 5 with a discussion and conclusion.

2 Higher-dimensional magnetic Skyrmions

A possible extension of planar magnetic Skyrmions can be realized by increasing the dimension of the base space and target space from two to three dimensions [30]. This amounts to a magnetization unit vector that would live in a 4-dimensional Cartesian space. For a physical realization, advanced concepts as synthetic dimensions must be considered, we will deal with this argument in Sec. 4. In symbols, the magnetization field is now a map $\mathbf{n} : \mathbb{R}^3 \rightarrow S^3$ where $\mathbf{n} = (n^1, n^2, n^3, n^4)$ and $\mathbf{n} \cdot \mathbf{n} = 1$. Let us consider the energy functional of the following form:

$$E[\mathbf{n}] = \sum_{\ell=0,1,2} E_{\ell}[\mathbf{n}] , \quad E_{\ell}[\mathbf{n}] = \int d^3x \mathcal{E}_{\ell}(\mathbf{n}) . \quad (2.1)$$

The Heisenberg exchange term is

$$\mathcal{E}_2(\mathbf{n}) = \frac{1}{2} \partial_i \mathbf{n} \cdot \partial_i \mathbf{n} . \quad (2.2)$$

As potential term \mathcal{E}_0 , we consider the generalized Zeeman potential:

$$\mathcal{E}_0(\mathbf{n}) = m^2 (1 - \mathbf{n} \cdot \mathbf{N})^p , \quad (2.3)$$

that is symmetric around the physical vacuum which is defined by

$$\lim_{r \rightarrow \infty} \mathbf{n} = \mathbf{N} , \quad (2.4)$$

and p is a positive real number defining the power of the potential. The latter condition (2.4) allows for the topological compactification of the base space \mathbb{R}^3 into S^3 , such that the vector field becomes a map $\mathbf{n} : S^3 \rightarrow S^3$. This leads to a nontrivial associated homotopy group $\pi_3(S^3) = \mathbb{Z} \ni B$, with B being the topological degree or so-called ‘‘baryon number’’. The topological degree can be computed as

$$B = \int_{\mathcal{B}} \mathcal{B} \, d^3x = \frac{1}{2\pi^2} \int \epsilon_{abcd} n^a \partial_1 n^b \partial_2 n^c \partial_3 n^d \, d^3x, \quad (2.5)$$

which is the pullback of the normalized volume form on the target S^3 by the field \mathbf{n} . Without loss of generality, as we will see in the next section, the vacuum can be chosen as $\mathbf{N} = (0, 0, 0, 1)^T$ and in any case the potential breaks the symmetry from $O(4)$ to $O(3)$. Finally, E_1 is the *new* energy term, which we include for the first time here, i.e. the 3-dimensional generalization of the planar DMI, which we shall discuss in the next section.

2.1 Generalized DM Interaction

2.1.1 Bloch-type DMI

Since we want to write down a generalization of the 2-dimensional DM term of Bloch-type,

$$\kappa \epsilon^{iab} \partial_i n^a n^b, \quad i = 1, 2, \quad a, b = 1, 2, 3, \quad (2.6)$$

for an $SO(4)$ vector, we choose the $SO(4)$ invariant tensor ϵ^{abcd} , which is totally antisymmetric and hence picks up a sign flip under cyclic permutations: $\epsilon^{abcd} = -\epsilon^{dabc}$. Now, in order to contract the ϵ tensor with the magnetization vector, we notice that the antisymmetric nature of the tensor allows us to contract only with one n . As for derivatives of n , we can contract also only with one ∂n , since we wish to avoid Derrick’s theorem by having less derivatives in the DM term than in the kinetic term (i.e. $(\partial n)^2$). Since the DM term

breaks rotational invariance already in the standard 2D formulation, there is no problem with contracting with a constant tensor, Θ . We thus arrive at

$$\mathcal{E}_1^{\text{Bloch}} := \kappa \epsilon_{abcd} \Theta^{abi} \partial_i n^c n^d, \quad (2.7)$$

where we raise and lower indices with Euclidean metrics. Clearly, Θ is a mixed tensor having two SO(4)-indices (a and b) and one spatial index i ; this may break rotational invariance.

In order to put the higher-dimensional DM term on the most general standard form, we use SO(4) and SO(3) transformations to simplify the tensor Θ as much as possible. Since Θ is contracted with the SO(4)-invariant tensor ϵ_{abcd} , we can from here on assume that it is antisymmetric in the SO(4)-indices a and b :

$$\Theta^{abi} = -\Theta^{bai}. \quad (2.8)$$

Performing simultaneously both orthogonal transformations, $R \in \text{SO}(4)$ and $r \in \text{SO}(3)$, we get

$$\begin{aligned} \mathcal{E}_1^{\text{Bloch}} &\rightarrow \kappa \epsilon_{abc'd'} \Theta^{abi'} r_{i'}^i \partial_i (R^c{}_c n^c) R^d{}_d n^d \\ &= \kappa \epsilon_{a'b'c'd'} R^a{}_e R^e{}_a R^b{}_f R^f{}_b \Theta^{abi'} r_{i'}^i \partial_i (R^c{}_c n^c) R^d{}_d n^d \\ &= \kappa \det(R) \epsilon_{abcd} R_e{}^a R_f{}^b \Theta^{efi'} r_{i'}^i \partial_i n^c n^d, \end{aligned} \quad (2.9)$$

from which we can read off the transformation on the tensor, Θ , as

$$\Theta^{abi} \rightarrow R_e{}^a R_f{}^b \Theta^{efi'} r_{i'}^i. \quad (2.10)$$

Writing this in matrix notation for the SO(4)-indices, we thus have a simple orthogonal transformation:

$$\Theta^i \rightarrow R^T \Theta^{i'} R r_{i'}^i. \quad (2.11)$$

Now since Θ^i is an antisymmetric real 4×4 matrix for each i , it has two conjugate pairs of pure imaginary eigenvalues. There is, however, no reason for the matrices to be aligned *a priori*. This means that we can only diagonalize one of the three matrices, say the $i = 3$ matrix:

$$\Theta^3 \sim \text{diag}(iA^3, -iA^3, iF^3, -iF^3), \quad (2.12)$$

with \sim denoting under an orthogonal transformation. Clearly, the determinant of Θ^3 is positive as it must be.

Now we should recall that the kinetic term \mathcal{E}_2 is invariant under the full $R \in \text{SO}(4)$ transformation, but the vacuum, and consequently the potential \mathcal{E}_0 is not. Notice that \mathbf{N}

will naturally transform under the rotation R . We may utilize the $\text{SO}(4)$ rotation to set the vacuum to be

$$\mathbf{N} = (0, 0, 0, 1)^T, \quad (2.13)$$

which is invariant only under the $\text{SO}(3)$ subgroup represented by $\rho \in \text{SO}(3) \subset \text{SO}(4)$ such that

$$R = \begin{pmatrix} \rho & 0 \\ 0 & 1 \end{pmatrix}. \quad (2.14)$$

Parametrizing the tensor Θ^{abi} as 3 matrices that transform under $\text{SO}(4)$, we have

$$\Theta^i = \frac{1}{2} \begin{pmatrix} 0 & A^i & B^i & D^i \\ -A^i & 0 & C^i & E^i \\ -B^i & -C^i & 0 & F^i \\ -D^i & -E^i & -F^i & 0 \end{pmatrix}, \quad (2.15)$$

the rotation ρ of Eq. (2.14) can only be used to diagonalize the submatrix consisting of A^i , B^i and C^i . Since the submatrix is 3×3 , it only possesses 1 purely imaginary pair of nonvanishing eigenvalues, as well as a zero eigenvalue. There is still no reason for the $\text{SO}(3)$ vectors to be aligned, so we can only diagonalize one of the Θ^i submatrices, say the $i = 3$ again. We thus arrive at

$$\Theta^\alpha = \frac{1}{2} \begin{pmatrix} 0 & A^\alpha & B^\alpha & D^\alpha \\ -A^\alpha & 0 & C^\alpha & E^\alpha \\ -B^\alpha & -C^\alpha & 0 & F^\alpha \\ -D^\alpha & -E^\alpha & -F^\alpha & 0 \end{pmatrix}, \quad \Theta^3 = \frac{1}{2} \begin{pmatrix} 0 & A^3 & 0 & D^3 \\ -A^3 & 0 & 0 & E^3 \\ 0 & 0 & 0 & F^3 \\ -D^3 & -E^3 & -F^3 & 0 \end{pmatrix}, \quad (2.16)$$

with $\alpha = 1, 2$. Using the $r \in \text{SO}(3)$ degrees of freedom, we can eliminate one symbol in Θ^α , by rotating it into the $i = 3$ direction; we may choose this to be $F^\alpha = 0$. We will denote this the standard form of the Θ tensor. One result of this computation is that the minimal degrees of freedom of the Θ tensor are 14.

At this point, it will be useful to identify a subset of the Θ tensor in standard form, that is invariant under a combined $\text{SO}(3) \subset \text{SO}(4)$ and $\text{SO}(3)$ symmetry. The transformation is again that of Eq. (2.10) with R of Eq. (2.14), it takes the form

$$\Theta^i \rightarrow \frac{1}{2} \begin{pmatrix} \rho^T \begin{pmatrix} 0 & A^j & B^j \\ -A^j & 0 & C^j \\ -B^j & -C^j & 0 \end{pmatrix} \rho & \rho^T \begin{pmatrix} D^j \\ E^j \\ F^j \end{pmatrix} \\ (-D^j & -E^j & -F^j) \rho & 0 \end{pmatrix} r_{ji}, \quad (2.17)$$

where both ρ and r belongs to $\text{SO}(3)$. From the above equation, it is clear that invariance requires the triplet A, B, C to transform under the adjoint representation of $\text{SO}(3)$ and

the triplet D, E, F to transform under the fundamental representation. This means that invariance under the combined rotation with the locking of the two $\text{SO}(3)$'s according to Eq. (2.14) with $\rho = r$, is attained by the tensor

$$\Theta^i = \frac{1}{2} \begin{pmatrix} 0 & \alpha\delta^{i3} & -\alpha\delta^{i2} & \beta\delta^{i1} \\ -\alpha\delta^{i3} & 0 & \alpha\delta^{i1} & \beta\delta^{i2} \\ \alpha\delta^{i2} & -\alpha\delta^{i1} & 0 & \beta\delta^{i3} \\ -\beta\delta^{i1} & -\beta\delta^{i2} & -\beta\delta^{i3} & 0 \end{pmatrix}, \quad (2.18)$$

with $\alpha, \beta \in \mathbb{R}$. We see that the invariant tensor only has two degrees of freedom. This invariant tensor can also be written in the basis of 't Hooft tensors as

$$\Theta^i = \frac{\alpha + \beta}{4} \eta^i + \frac{\alpha - \beta}{4} \bar{\eta}^i, \quad (2.19)$$

where the 't Hooft tensors are given by

$$\begin{aligned} \eta^1 &= \begin{pmatrix} 0 & \tau^1 \\ -\tau^1 & 0 \end{pmatrix}, & \eta^2 &= \begin{pmatrix} 0 & -\tau^3 \\ \tau^3 & 0 \end{pmatrix}, & \eta^3 &= \begin{pmatrix} i\tau^2 & 0 \\ 0 & i\tau^2 \end{pmatrix}, \\ \bar{\eta}^1 &= \begin{pmatrix} 0 & -i\tau^2 \\ -i\tau^2 & 0 \end{pmatrix}, & \bar{\eta}^2 &= \begin{pmatrix} 0 & -\mathbf{1}_2 \\ \mathbf{1}_2 & 0 \end{pmatrix}, & \bar{\eta}^3 &= \begin{pmatrix} i\tau^2 & 0 \\ 0 & -i\tau^2 \end{pmatrix}. \end{aligned} \quad (2.20)$$

One may also consider the simplified tensor

$$\Theta^{abi} = \Gamma^a \delta^{bi}, \quad (2.21)$$

which clearly is not antisymmetric in the $\text{SO}(4)$ -indices a and b . Anti-symmetrizing them gives

$$\Theta^{abi} = \frac{1}{2} (\Gamma^a \delta^{bi} - \Gamma^b \delta^{ai}), \quad (2.22)$$

which written out in matrix form reads

$$\Theta^i = \frac{1}{2} \begin{pmatrix} 0 & \Gamma^1 \delta^{2i} - \Gamma^2 \delta^{1i} & \Gamma^1 \delta^{3i} - \Gamma^3 \delta^{1i} & -\Gamma^4 \delta^{1i} \\ \Gamma^2 \delta^{1i} - \Gamma^1 \delta^{2i} & 0 & \Gamma^2 \delta^{3i} - \Gamma^3 \delta^{2i} & -\Gamma^4 \delta^{2i} \\ \Gamma^3 \delta^{1i} - \Gamma^1 \delta^{3i} & \Gamma^3 \delta^{2i} - \Gamma^2 \delta^{3i} & 0 & -\Gamma^3 \delta^{3i} \\ \Gamma^4 \delta^{1i} & \Gamma^4 \delta^{2i} & \Gamma^4 \delta^{3i} & 0 \end{pmatrix}. \quad (2.23)$$

This tensor is contained within the standard form of Θ by identifying

$$\begin{aligned} A^i &= \left(-\Gamma^2, \Gamma^1, \sqrt{(\Gamma^1)^2 + (\Gamma^2)^2} \right), \\ B^\alpha &= (-\Gamma^3, 0), \\ C^\alpha &= (0, -\Gamma^3), \\ D^\alpha &= (-\Gamma^4, 0), \\ E^\alpha &= (0, -\Gamma^4), \\ F^3 &= -\Gamma^4, \end{aligned} \quad (2.24)$$

and $F^\alpha = 0$ with $\alpha = 1, 2$. Considering an invariant subset of this tensor under the combined SO(3) rotation (2.10) yields

$$\Theta^{abi} \rightarrow \frac{1}{2}(R^T \Gamma)^a \delta^{bi} - \frac{1}{2}(R^T \Gamma)^b \delta^{ai}. \quad (2.25)$$

Using now the rotation R of Eq. (2.14), it is clear that invariance is only preserved if

$$\Gamma_{\text{inv}}^a = -\beta \delta^{a4}, \quad (2.26)$$

in agreement with the invariant tensor on the standard form (2.18).

Another simplified tensor may be constructed by taking the ‘‘Hodge dual’’ of the Θ tensor. In order to dualize in 4 dimensions, we extend the index i to $i = 1, 2, 3, 4$, but with the derivative $\partial_4 = 0$. In this case, we have

$$\Theta^{abi} = \frac{1}{2} \epsilon^{abik} \Psi^k, \quad (2.27)$$

where the factor of $1/2$ is introduced for convenience. This tensor is also contained within the standard form of Θ by identifying

$$\begin{aligned} A^3 &= \Psi^4, \\ B^\alpha &= (0, -\Psi^4), \\ C^\alpha &= (\Psi^4, 0), \\ D^\alpha &= (0, \Psi^3), \\ E^\alpha &= (-\Psi^3, 0), \\ F^\alpha &= (\Psi^2, -\Psi^1), \end{aligned} \quad (2.28)$$

where this time we have chosen $A^\alpha = 0$. It is again clear that only a subset of this tensor is an invariant under the transformation (2.10) and it is given by

$$\Psi^a = \alpha \delta^{a4}. \quad (2.29)$$

Interestingly, the invariant of this tensor corresponds to the α -part of the invariant tensor on standard form (2.18), whereas the invariant tensor (2.26) corresponds to the β -part.

2.1.2 Néel-type DMI

In two dimensions the DM term can equivalently take a different form, known as the DMI of Néel type:

$$\kappa(\mathbf{n} \cdot \nabla n^3 - n^3 \nabla \cdot \mathbf{n}), \quad (2.30)$$

with $\nabla = (\partial_1, \partial_2, 0)$ and $\mathbf{n} = (n^1, n^2, n^3)$, which is due to the Rashba spin-orbit coupling (SOC), whereas the Bloch-type DMI (2.6) corresponds to the Dresselhaus SOC. Although, this DM term looks quite different from the Bloch type (2.6), the Néel-type DMI is simply obtained from the Bloch-type DMI by performing an $\text{SO}(2) \subset \text{SO}(3)$ rotation of the magnetization vector $(n^1, n^2, n^3) \mapsto (n^2, -n^1, n^3)$ and keeping the derivative vector fixed. The generalization of the above 2-dimensional DM term to a higher-dimensional DM term, however, is straightforward and somewhat different³:

$$\mathcal{E}_1^{\text{Néel}} = \kappa(n^4 \nabla \cdot \mathbf{n} - \mathbf{n} \cdot \nabla n^4), \quad (2.31)$$

where now $\nabla = (\partial_1, \partial_2, \partial_3, 0)$ and $\mathbf{n} = (n^1, n^2, n^3, n^4)$. The symmetry properties are also quite clear and simple in this case, since the inner product is preserved by a combined rotation in $\rho \in \text{SO}(3) \subset \text{SO}(4)$ (see Eq. (2.14)) and $r \in \text{SO}(3)$, with the symmetry-locking mechanism again given by $\rho = r$.

In fact, by a closer inspection it is clearly $\text{SO}(3)$ invariant, as it is simply equal to the tensor (2.27) with Ψ^a of Eq. (2.29), corresponding to the α -part of the $\text{SO}(3)$ invariant tensor (2.18). Indeed, a simple calculation shows that

$$\frac{1}{2} \kappa \epsilon_{abcd} \epsilon^{abi4} \partial_i n^c n^d = \kappa (\delta_c^i \delta_d^4 - \delta_c^4 \delta_d^i) \partial_i n^c n^d = \kappa (n^4 \nabla \cdot \mathbf{n} - \mathbf{n} \cdot \nabla n^4), \quad (2.32)$$

which is exactly Eq. (2.31).

2.1.3 Axially symmetric DMI

The Néel-type DM term (2.31) already possesses $\text{SO}(3)$ symmetry, whereas the general Bloch-type generalization (2.7) does not. Considering the Θ tensor (2.15), we can relax the spherical (i.e. $\text{SO}(3)$) symmetry restriction to only an axial symmetry. Using the transformation (2.10), but with the $\text{SO}(4)$ transformation, i.e.,

$$R = \begin{pmatrix} \rho' & 0 \\ 0 & \mathbf{1}_2 \end{pmatrix}, \quad (2.33)$$

with $\rho' \in \text{SO}(2)$, $\mathbf{1}_2$ being the 2×2 unit matrix, and with the $\text{SO}(2) \subset \text{SO}(3)$ spatial rotation

$$r = \begin{pmatrix} \rho' & 0 \\ 0 & 1 \end{pmatrix}, \quad (2.34)$$

³Often the opposite sign of the Néel-type DMI is used, which can be reached from the Bloch-type DMI simply by rotating the opposite way in the 1-2 plane: $(n^1, n^2, n^3) \mapsto (-n^2, n^1, n^3)$, or alternatively by flipping the sign of κ .

we can find an axially invariant Θ tensor of the form

$$\Theta^i = \frac{1}{2} \begin{pmatrix} 0 & 0 & \gamma\delta^{i1} & \eta\delta^{i1} \\ 0 & 0 & \gamma\delta^{i2} & \eta\delta^{i2} \\ -\gamma\delta^{i1} & -\gamma\delta^{i2} & 0 & F^3\delta^{i3} \\ -\eta\delta^{i1} & -\eta\delta^{i2} & -F^3\delta^{i3} & 0 \end{pmatrix}. \quad (2.35)$$

The two vectors proportional to γ and η are invariants under the combined $\text{SO}(2)$ rotation in the x - y plane, but (F^1, F^2) still transforms, so we must set them to zero.

2.2 Spherically symmetric magnetic Skyrmions

In order to construct a spherically symmetric magnetic Skyrmion, we necessarily need to consider only the $\text{SO}(3)$ invariant subtensors, which for the Bloch-type DM term corresponds to the α and β parts of Eq. (2.18). Considering the model that closest resembles the 2D magnetic Skyrmion, we take the energy density to be

$$\mathcal{E} = \mathcal{E}_2 + \mathcal{E}_1 + \mathcal{E}_0. \quad (2.36)$$

The kinetic term, \mathcal{E}_2 , is invariant under $\text{O}(4)_{\text{internal}} \times \text{O}(3)_{\text{space}} \times T_3$ symmetry, which is broken down to $\text{O}(3)_{\text{internal}} \times \text{O}(3)_{\text{space}} \times T_3$ by the potential, \mathcal{E}_0 , where T_3 are spatial translations and \times is the semi-direct product. The DM term, \mathcal{E}_1 , further breaks the symmetry which is clear from the derivation in Sec. 2.1.1, viz. the internal symmetry is locked with the spatial rotations, yielding the symmetry of the theory

$$G = \text{O}(3)_{\text{diag}} \times T_3. \quad (2.37)$$

The hedgehog Ansatz with an azimuthal rotation by δ is given by the map

$$\mathbf{n} = \begin{pmatrix} \sin \chi \sin \theta \cos(\phi + \delta) \\ \sin \chi \sin \theta \sin(\phi + \delta) \\ \sin \chi \cos \theta \\ \cos \chi \end{pmatrix}, \quad \chi, \theta \in [0, \pi], \quad \phi \in [0, 2\pi), \quad (2.38)$$

with (r, θ, ϕ) being the normal spherical coordinates and $\chi(r)$ the radial profile function. The energy densities for the kinetic and potential terms are independent of δ and read

$$\mathcal{E}_2 = \frac{1}{2}(\chi')^2 + \frac{\sin^2 \chi}{r^2}, \quad (2.39)$$

$$\mathcal{E}_0 = m^2(1 - \cos \chi)^p, \quad p > 0, \quad (2.40)$$

with $\chi' := \partial_r \chi(r)$. We typically take $p = 1$ or alternatively $p = \frac{3}{2}$ or $p = 2$.

More interesting is the SO(3)-invariant DM term (2.18), which under the hedgehog Ansatz reduces to

$$\begin{aligned} \mathcal{E}_1^{\text{Bloch}} = & \kappa\alpha \cos \delta \left(\sin^2 \theta \chi' + \frac{(1 + \cos^2 \theta) \sin 2\chi}{2r} \right) + \kappa\alpha \left(\cos^2 \theta \chi' + \frac{\sin^2 \theta \sin 2\chi}{2r} \right) \\ & + 2\kappa\beta \sin \delta \frac{\cos \theta \sin^2 \chi}{r}. \end{aligned} \quad (2.41)$$

The β -part of the term vanishes upon integration of $d\theta$ (i.e. $\int_0^\pi \sin 2\theta d\theta = 0$). We notice that the term becomes spherically symmetric when $\delta = 0$:

$$\mathcal{E}_1^{\text{Bloch}} = \kappa\alpha \left(\chi' + \frac{\sin 2\chi}{r} \right). \quad (2.42)$$

Integrating instead (2.41) over θ , we obtain

$$\int \mathcal{E}_1^{\text{Bloch}} \sin \theta d\theta = \frac{2\kappa\alpha}{3} (1 + 2 \cos \delta) \left(\chi' + \frac{\sin 2\chi}{r} \right). \quad (2.43)$$

Since the DM term contributes as negative energy, maximizing its prefactor corresponds to minimizing the energy, which is quickly seen to occur at $\delta = 0$, the symmetric point. We also absorb α into κ and thus arrive at

$$\mathcal{E}_1^{\text{Bloch}} = \kappa \left(\chi' + \frac{\sin 2\chi}{r} \right). \quad (2.44)$$

If we instead consider the generalized Néel-type DM term (2.31), we obtain under the hedgehog Ansatz the exactly the α -part of the Bloch-type DM (see Eq. (2.41)), as expected. The symmetry is enhanced when $\delta = 0$ and in that case the above density reduces to

$$\mathcal{E}_1^{\text{Néel}} = \kappa \left(\chi' + \frac{\sin 2\chi}{r} \right). \quad (2.45)$$

We thus conclude that both the Bloch-type and Néel-type DMIs give under the hedgehog Ansatz (2.38) rise to the same DM term, i.e. $E_1^{\text{Bloch}} = E_1^{\text{Néel}} \equiv E_1$, which is schematically very similar to the polar symmetric one in two dimensions. A summary is presented in Tab. 1 for the reader's convenience.

	α -part	β -part	sph. sym.
Bloch-type	(2.29)	(2.26)	(2.44) ($\beta = 0$)
Néel-type	(2.29)	0	(2.45)

Table 1: Bloch-type and Néel-type DMIs. Note that the β -part of the Bloch-type DM vanishes in the spherically symmetric case.

The total energy ($E = \int \mathcal{E} d^3x$) of the higher-dimensional magnetic Skyrme model under the hedgehog Ansatz (2.38) is thus given by

$$E = 4\pi \int \left[\frac{1}{2} r^2 (\chi')^2 + \sin^2 \chi + \kappa (r^2 \chi' + r \sin 2\chi) + m^2 r^2 (1 - \cos \chi)^p \right] dr, \quad (2.46)$$

which gives rise to the following Euler-Lagrange equation

$$\text{eom}_\chi = \chi'' + \frac{2}{r} \chi' - \frac{\sin 2\chi}{r^2} + \frac{4\kappa \sin^2 \chi}{r} - pm^2 (1 - \cos \chi)^{p-1} \sin \chi = 0. \quad (2.47)$$

It is well known that using a scaling argument, we can without loss of generality reduce the parameters of the theory from 2 to 1, by rescaling lengths and choosing a suitable energy unit. Rescaling $r \rightarrow \lambda r$, we thus arrive at

$$E_\lambda = \lambda E_2 + \lambda^2 E_1 + \lambda^3 E_0. \quad (2.48)$$

Derrick's theorem [29] prevents stable solitonic solutions to this theory if all $E_{2,1,0}$ were positive definite. However, since E_1 can be negative, stability can be attained. From this argument, it is clear that we could remove the potential term E_0 and, in principle, still have stable solutions. We therefore scale away κ with $\lambda = \kappa^{-1}$ and energies are measured in units of $\lambda = \kappa^{-1}$. Absorbing λ into the mass parameter, we arrive at

$$E = \frac{4\pi}{\kappa} \int \left[\frac{1}{2} r^2 (\chi')^2 + \sin^2 \chi + (r^2 \chi' + r \sin 2\chi) + m^2 r^2 (1 - \cos \chi)^p \right] dr. \quad (2.49)$$

Since $\kappa = 0$ cannot give rise to stable solitons, it is no problem to divide the energy functional by κ . The equation of motion is just Eq. (2.47) with κ set to unity.

Finally, the topological charge is given by Eq. (2.5), which under the Ansatz (2.38) simplifies to

$$B = \int \mathcal{B} d^3x = -\frac{2}{\pi} \int \sin^2(\chi) \chi' dr = \frac{2}{\pi} \int_0^\pi \sin^2 \chi d\chi = 1, \quad (2.50)$$

where we have used the boundary conditions $\chi(0) = \pi$ and $\chi(\infty) = 0$.

2.2.1 Full equations of motion

Using the principle of symmetric criticality, the equation of motion (2.47) solves the full equations of motion, if and only if the Ansatz is compatible with the symmetries of the full theory. Nevertheless, the full equations of motion serve as a consistency check of the Ansatz and in the 2D case, they furthermore determine the phase parameter δ .

The full equation of motion reads

$$\partial_i^2 n^a + 2\kappa \epsilon_{abcd} \Theta^{bc} \partial_i n^d + pm^2 (1 - \mathbf{n} \cdot \mathbf{N})^{p-1} N^a - \lambda n^a = 0, \quad (2.51)$$

where λ is a Lagrange multiplier that can be determined as

$$\lambda = \mathbf{n} \cdot \partial_i^2 \mathbf{n} - 2\kappa \epsilon_{abcd} \Theta^{abi} \partial_i n^c n^d + pm^2 (1 - \mathbf{n} \cdot \mathbf{N})^{p-1} \mathbf{n} \cdot \mathbf{N}. \quad (2.52)$$

Inserting the spherical Ansatz (2.38), Eq. (2.51) reduces to

$$\frac{\partial \mathbf{n}}{\partial \chi} \times \text{eom}_\chi + \sin\left(\frac{\delta}{2}\right) \mathbf{V} + \sin^2\left(\frac{\delta}{2}\right) \mathbf{W} = 0, \quad (2.53)$$

with eom_χ of Eq. (2.47) and where we have defined

$$\mathbf{V} = 2\kappa \begin{pmatrix} -\frac{1}{2} \sin \chi \sin \theta \left[3 \sin\left(\frac{\delta}{2} + \phi\right) + \sin\left(\frac{3\delta}{2} + \phi\right) \right] \chi' \\ \frac{1}{2} \sin \chi \sin \theta \left[3 \cos\left(\frac{\delta}{2} + \phi\right) + \cos\left(\frac{3\delta}{2} + \phi\right) \right] \chi' \\ 0 \\ 0 \end{pmatrix}, \quad (2.54)$$

$$\mathbf{W} = 2\kappa \begin{pmatrix} n^1 \left[-(1 + \cos^2 \theta) \frac{\sin 2\chi}{r} + \cos(2\theta) \chi' \right] \\ n^2 \left[-(1 + \cos^2 \theta) \frac{\sin 2\chi}{r} + \cos(2\theta) \chi' \right] \\ -n^3 \left[(1 + \cos^2 \theta) \frac{\sin 2\chi}{r} + 2 \sin^2(\theta) \chi' \right] \\ 2(1 + \cos^2 \theta) \frac{\sin^3 \chi}{r} \end{pmatrix}, \quad (2.55)$$

which demonstrates that Eq. (2.47) is consistently solving the full equations of motion if and only if $\delta = 0$. Unlike the situation in 2D, here the solution to the full equations of motion uniquely determine the rotation phase of the Ansatz to be $\delta = 0$. On the other hand, in the standard 2D magnetic Skyrmion case, there are two solutions corresponding to a rotation in the plane by $\delta = \frac{\pi}{2}$ and $\delta = -\frac{\pi}{2}$, with the former being the minimum of the energy and the latter the maximum. In this case, the generalized DMI is only spherically symmetric when $\delta = 0$ and therefore $\text{eom}_\chi = 0$ only solves the full equations of motion for that value of δ .

2.2.2 Numerical Skyrmion solutions

We will now compute a spectrum of numerical solutions for the 3D generalization of the Skyrmion with a higher-dimensional DM term that is $\text{SO}(3)$ -invariant: namely the α -invariant part of Eq. (2.18). We utilize the rescaling of lengths, so that the coefficient of the higher-dimensional DMI is unity, but the energy is measured in units of inverse κ , see Eq. (2.49). We solve the equation of motion (2.47) with κ set to unity (under the rescaled scheme) using gradient flow. The gradient flow method is suitable for the stable 3D Skyrmions and is easier to use than a shooting method due to the large sizes of the Skyrmions, when m is small. We have cross-checked the solutions using the shooting algorithm and confirmed their accuracy.

Fig. 1 shows the profile functions of the solutions for the full range of parameters, i.e. $m \in (0, m_{\text{crit}}]$ in the rescaled lengths where κ only enters as the (inverse) unit of

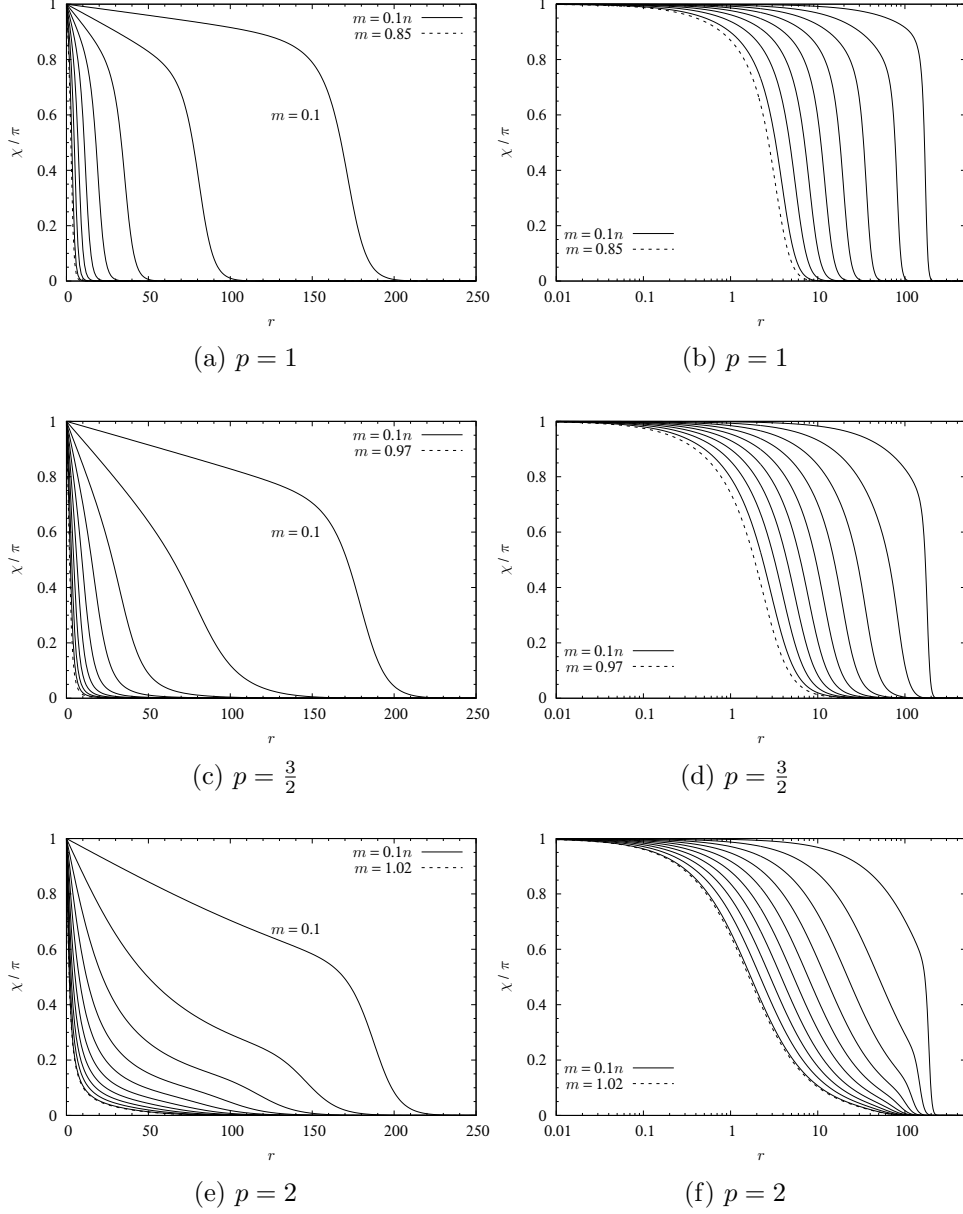


Figure 1: Profile functions for 3D magnetic Skyrmions with higher-dimensional SO(3)-invariant DM term. Left panels (a,c,e) show the profile on a regular scale and the right panels (b,d,f) on a log scale. The m_{crit} solution is shown with a dashed line. The rows of panels correspond to the potential power parameter $p = 1, \frac{3}{2}, 2$. No solutions exist for $m > m_{\text{crit}}$ nor for $m = 0$.

p	m_{crit}
1	0.85
$\frac{3}{2}$	0.97
2	1.02

Table 2: The critical mass parameter m_{crit} for the potential with $p = 1, \frac{3}{2}, 2$. No solutions exist for $m > m_{\text{crit}}$, but solutions exist in the interval $m \in (0, m_{\text{crit}}]$.

energy. There exist no solution for $m > m_{\text{crit}}$ and for the 3 potential power parameters, $p = 1, \frac{3}{2}, 2$, we give the approximate critical masses in Tab. 2. Notice also that no 3D magnetic Skyrmion solution exists for $m = 0$, see below though. We can understand the critical mass as follows. For fixed DM-term coefficient (in the effective rescaling of parameters in the theory), the only theory parameter is m . For small m , the DM term can stabilize the soliton, whereas for large m , the pressure to collapse the soliton eventually becomes too large, and hence no soliton exists.

As can be inferred from Derrick scaling, the largest 3D magnetic Skyrmion solution is the one with the smallest mass and the smallest ones are the $m = m_{\text{crit}}$ ones, see the approximate sizes in Fig. 5(a).

Fig. 2 shows the energy densities (left panels) and topological charge densities (right panels). The left panels show the total energy densities for the full range of the mass parameter, m , using black lines and the DM contribution to the energy density using red lines. The densities are weighted by r^2 to make the features of the densities better visible. The 3 rows of the figure correspond to different values of the potential power parameter, $p = 1, \frac{3}{2}, 2$.

2.2.3 Restricted model

If we consider a rescaling of lengths $r \rightarrow \lambda r$ with $\lambda = \frac{\kappa}{m^2}$, we obtain a theory where the coefficients in front of the DM term and the potential term both equal $\frac{\kappa^2}{m^2}$, whereas the coefficient of the kinetic term remains unity (the energy unit is now $\frac{\kappa}{m^2}$). Now, taking $\kappa \gg m > 0$, the kinetic term becomes negligible and we arrive at the restricted version of the model,

$$\begin{aligned}
 E^{\text{restricted}} &= \frac{\kappa^2}{m^4} E_1 + \frac{\kappa^3}{m^6} E_0 \\
 &= \frac{4\pi\kappa^3}{m^4} \int [r^2 \chi' + r \sin 2\chi + r^2(1 - \cos \chi)^p] dr,
 \end{aligned} \tag{2.56}$$

which has the algebraic and explicit equation of motion

$$r = \frac{4 \sin \chi}{2^{p-1} p \sin^{2(p-1)} \left(\frac{\chi}{2}\right)}. \tag{2.57}$$

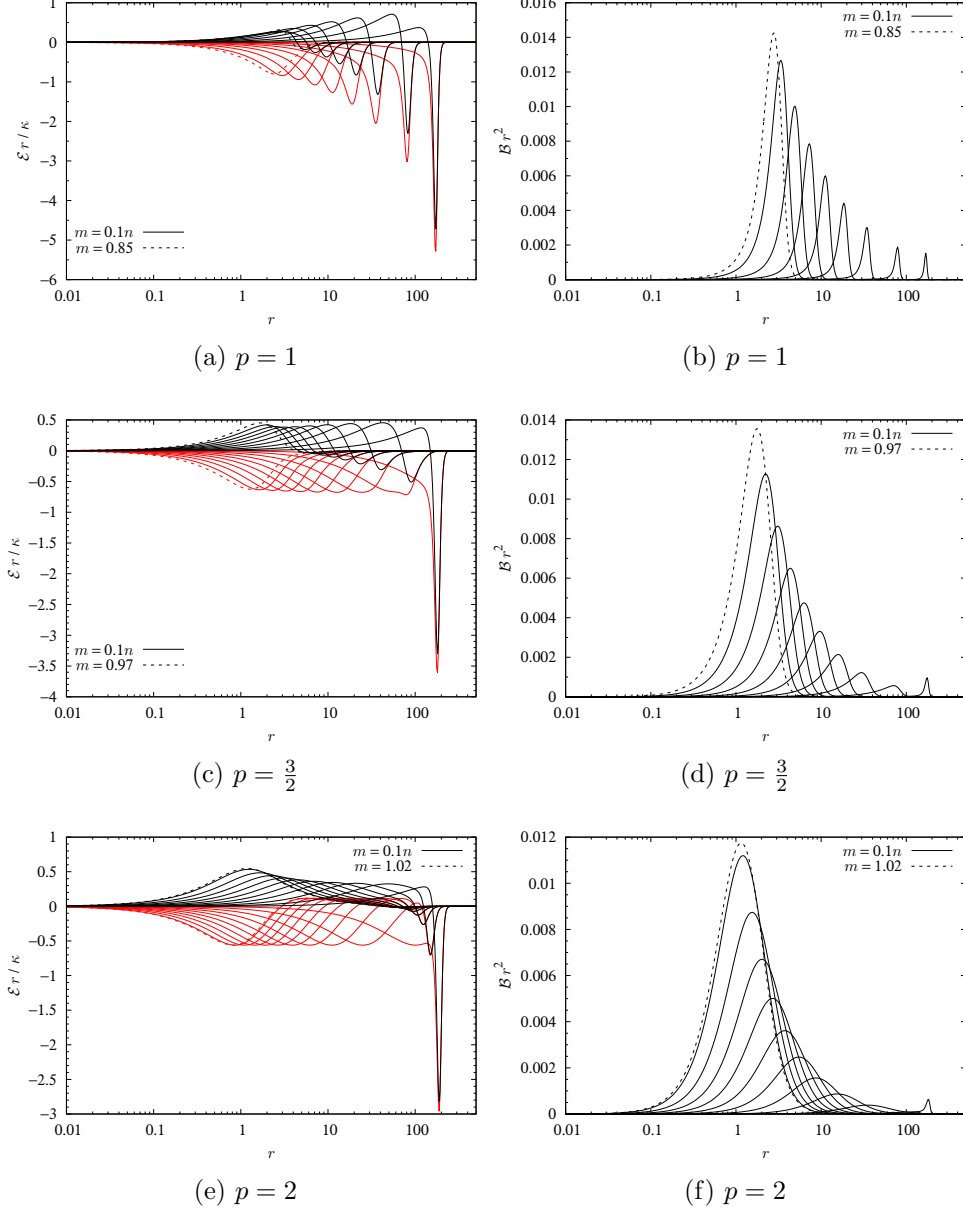


Figure 2: Energy density and topological charge density for 3D magnetic Skyrmions with higher-dimensional $SO(3)$ -invariant DM term. Left panels (a,c,e) show the total energy densities weighted with r (for visualization purposes) as black lines and the DM contribution as red lines. Right panels (b,d,f) show the topological charge density, weighted with r^2 . The m_{crit} solution is shown with a dashed line. The rows of panels correspond to the potential power parameter $p = 1, \frac{3}{2}, 2$. No solutions exist for $m > m_{\text{crit}}$ nor for $m = 0$.

This solution is formally identical with the restricted 2D magnetic Skyrmion solution of Ref. [52]. In particular, we have

$$p = 1 : \quad \chi(r) = \pi - \arcsin\left(\frac{r}{4}\right), \quad (2.58)$$

$$p = \frac{3}{2} : \quad \chi(r) = 2 \arccos\left(\frac{3\sqrt{2}r}{16}\right), \quad (2.59)$$

$$p = 2 : \quad \chi(r) = 2 \arctan\left(\frac{r}{2}\right). \quad (2.60)$$

2.2.4 The anti-Skyrmion

In the 2-dimensional magnetic Skyrme model, the anti-Skyrmion is unstable. It is worthwhile to discuss the anti-Skyrmion in this higher-dimensional model, since it is somewhat different from the 2-dimensional case. The simplest way to obtain the anti-Skyrmion is to flip the polar angle $\phi \rightarrow -\phi$ in Eq. (2.38). The β -part of the DMI still vanishes, but the α -part changes to

$$\int \mathcal{E}_1^{\overline{\text{Sk}}} \sin \theta \, d\theta = \frac{2\kappa}{3} \left[(1 - \cos \delta) \frac{\sin 2\chi}{r} + (1 + 2 \cos \delta) \chi' \right]. \quad (2.61)$$

Integrating by parts and assuming $m > 0$ such that the boundary term vanishes, we can show that

$$\int \mathcal{E}_1^{\overline{\text{Sk}}} \sin \theta \, d\theta = \frac{2\kappa}{3} [\cos \delta (3 - \sin^2 \chi) + 2 \sin^2 \chi] \chi', \quad (2.62)$$

which should be compared to

$$\int \mathcal{E}_1^{\text{Sk}} \sin \theta \, d\theta = \frac{2\kappa}{3} [(1 + 2 \cos \delta) 2 \sin^2(\chi)] \chi', \quad (2.63)$$

for the Skyrmion. For the Skyrmion the prefactor is clearly maximized by $\delta = 0$. This is also the case for the anti-Skyrmion, which can be seen by comparing the case with $\kappa > 0$ and $\delta = 0$ to the case of $\kappa < 0$ and $\delta = \pi$, which are the most positive and the most negative values of the square brackets. So although the anti-Skyrmion exists, it will have a smaller coefficient of the DM term and hence a larger energy than the Skyrmion for $\delta := 0$. This can be seen by comparing the DMI for the anti-Skyrmion to the Skyrmion in the following form:

$$\int \mathcal{E}_1^{\text{Sk}} \sin \theta \, d\theta = 2\kappa \left(\frac{\sin 2\chi}{r} + \chi' \right), \quad (2.64)$$

$$\int \mathcal{E}_1^{\overline{\text{Sk}}} \sin \theta \, d\theta = \int \mathcal{E}_1^{\text{Sk}} \sin \theta \, d\theta - 2\kappa \frac{\sin 2\chi}{r}. \quad (2.65)$$

Since the term $-\frac{\sin 2\chi}{r}$ is positive for small r where $\chi > \pi/2$, it will increase the energy of the anti-Skyrmion with respect to the Skyrmion (more than it will decrease the energy for $\chi > \pi/2$, since the term will be small for large r), leaving the Skyrmion the stable soliton in the theory.

2.3 Magnetic sphalerons

Considering again the rescaling of lengths as $r \rightarrow \lambda r$, we get Eq. (2.48). By identifying the characteristic radius of the soliton as R and approximating the integrals of the energy functional by constants as

$$\lambda E_2 = c_2 R, \quad \lambda^2 E_1 = -c_1 \kappa R^2, \quad \lambda^3 E_0 = c_0 m^2 R^3, \quad (2.66)$$

we can write the approximate energy functional as a function of the soliton size, R :

$$E(R) = c_2 R - c_1 \kappa R^2 + c_0 m^2 R^3, \quad (2.67)$$

Choosing energy and length units more convenient for the problem at hand, we can write the above function as

$$E(\tilde{R}) = \frac{c_2^{\frac{3}{2}}}{\sqrt{c_0 m}} \left[\tilde{R} - \tilde{\kappa} \tilde{R}^2 + \tilde{R}^3 \right], \quad \tilde{R} = \frac{R}{R_0} = \sqrt{\frac{c_0}{c_2}} m R, \quad (2.68)$$

where we have defined

$$\tilde{\kappa} = \frac{\kappa c_1}{\sqrt{c_0 c_2 m}}. \quad (2.69)$$

The virial law is now given by

$$E'(\tilde{R}) = \frac{c_2^{\frac{3}{2}}}{\sqrt{c_0 m}} \left[1 - 2\tilde{\kappa} \tilde{R} + 3\tilde{R}^2 \right] = 0. \quad (2.70)$$

In contradistinction to the 2-dimensional magnetic Skyrmion case, in 3 dimensions there are two solutions to the virial equation:

$$R_{\pm} = \frac{\tilde{\kappa} \pm \sqrt{\tilde{\kappa}^2 - 3}}{3} R_0. \quad (2.71)$$

Clearly, there are no solutions if $\tilde{\kappa} < \sqrt{3}$, in which case the DM term is not strong enough to stabilize a soliton solution. However, as soon as $\tilde{\kappa}$ is big enough, two solutions exist: the large one is the 3D magnetic Skyrmion and we call the small one a magnetic sphaleron. Although we cannot expect $c_{2,1,0}$ to be truly constants for all values of the parameters of the

energy functional, we assume their dependence to be mild. Nevertheless, it is illuminating to expand in small m :

$$R_- = \frac{c_2}{2c_1\kappa} + \frac{3c_0c_2^2m^2}{8c_1^3\kappa^3} + \mathcal{O}(m^4), \quad (2.72)$$

$$R_+ = \frac{2c_1\kappa}{3c_0m^2} - \frac{c_2}{2c_1\kappa} - \frac{3c_0c_2^2m^2}{8c_1^3\kappa} + \mathcal{O}(m^4). \quad (2.73)$$

The solution corresponding to R_- , which is the magnetic sphaleron, tends to a finite size as m tends to zero, whereas the solution corresponding to R_+ diverges as $m \rightarrow 0$. The finite size of R_- for $m = 0$ shows that the massless magnetic sphaleron is stabilized exclusively by the balance of the kinetic and the DM term. The latter solution, R_+ , is the 3D magnetic Skyrmion. Since R_+ diverges in the limit of $m \rightarrow 0$, the Skyrmion disappears in that limit.

2.3.1 Numerical sphaleron solutions

We solve the equation of motion (2.47) with κ set to unity (under the rescaled scheme) using the shooting method. The reason for changing the algorithm from gradient flow to the shooting method, is that the magnetic sphaleron solutions are unstable, which makes the gradient flow method easily flow to the stable 3D magnetic Skyrmions instead. Linearizing the equation of motion (2.47), we find that at small distances $r \ll 1$, the profile function behaves like $\chi = \pi - cr + \mathcal{O}(r^2)$. We use c as the shooting parameter and require $\chi(r_{\max}) = 0$, with a suitably large r_{\max} . The typical values of the shooting parameter for the magnetic sphalerons are in the range $c \approx 2 \div 6$.

Fig. 3 shows the profile functions of the solutions for the full range of parameters, i.e. $m \in [0, m_{\text{crit}}]$ in the rescaled lengths where κ only enters as the (inverse) unit of energy. As in the 3D magnetic Skyrmion case, there exist no solution for $m > m_{\text{crit}}$, as can also be seen from Eq. (2.71). The upper bound on m corresponds to the lower bound on $\tilde{\kappa} \geq \sqrt{3}$ and when satisfied, both the 3D magnetic Skyrmion and the magnetic sphaleron exist.

Interestingly, we can see that increasing the potential (mass) parameter, m , inflates the bulk of the soliton but suppresses the tail for $p = 1$. For $p > 1$, the tail is not suppressed in the same way, since the potential is not simply giving rise to an exponential behavior, but is nonlinearly suppressing the tail.

Fig. 4 shows the energy densities and topological charge densities. The left panels show the total energy densities with black lines and the DM contribution with red lines. The 3 rows of the figure correspond to different values of the potential power parameter, $p = 1, \frac{3}{2}, 2$.

The sizes of the Skyrmions given in Fig. 5(a) are found simply by determining the radius where the profile function χ is half-way between the anti-vacuum and the vacuum, i.e. $\chi(r) = \frac{\pi}{2}$. The energies are shown in Fig. 5(b) with positive sign for the sphaleron

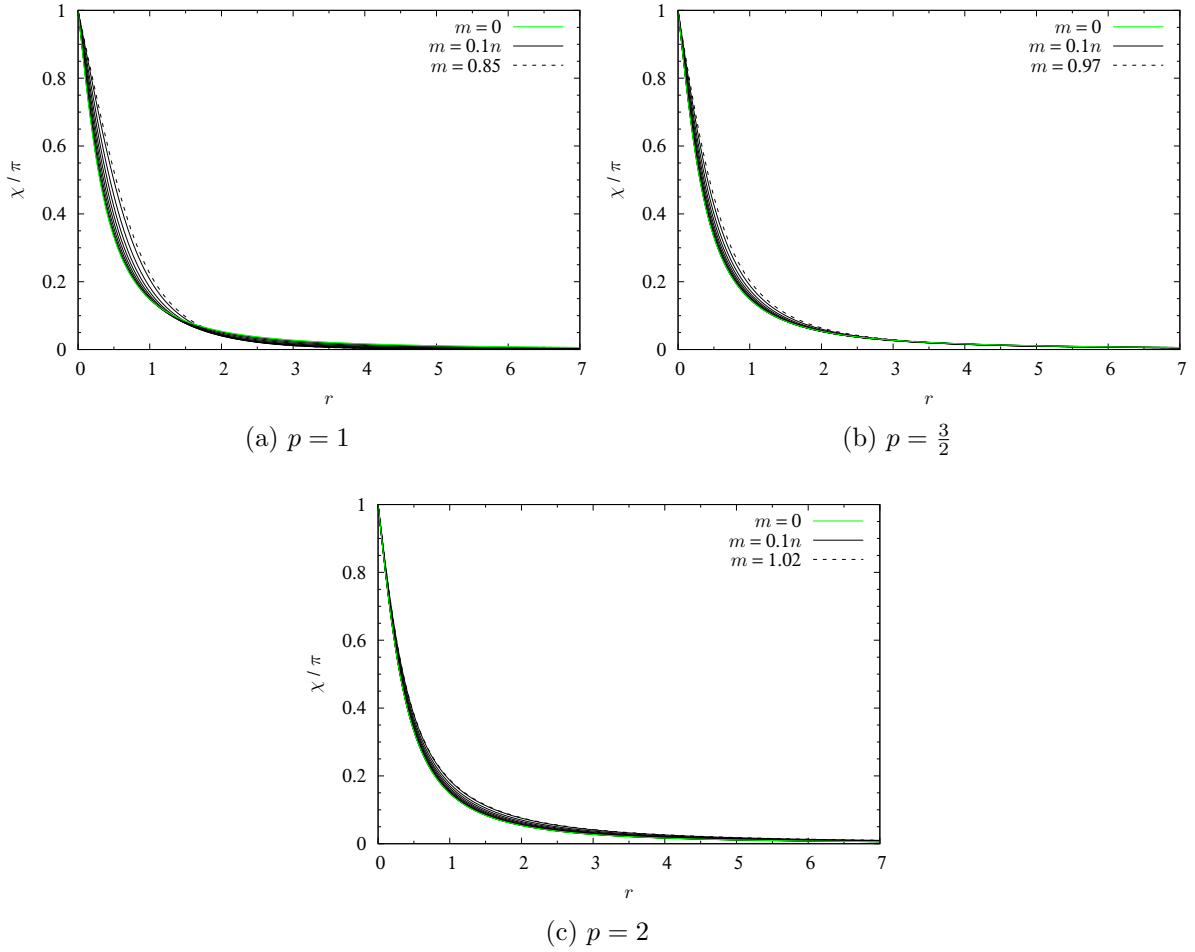


Figure 3: Profile functions for magnetic sphalerons with higher-dimensional SO(3)-invariant DM term, for (a) $p = 1$, (b) $p = \frac{3}{2}$ and (c) $p = 2$. The $m = 0$ solution is shown with a green line and the m_{crit} solution with a dashed line. No solutions exist for $m > m_{\text{crit}}$.

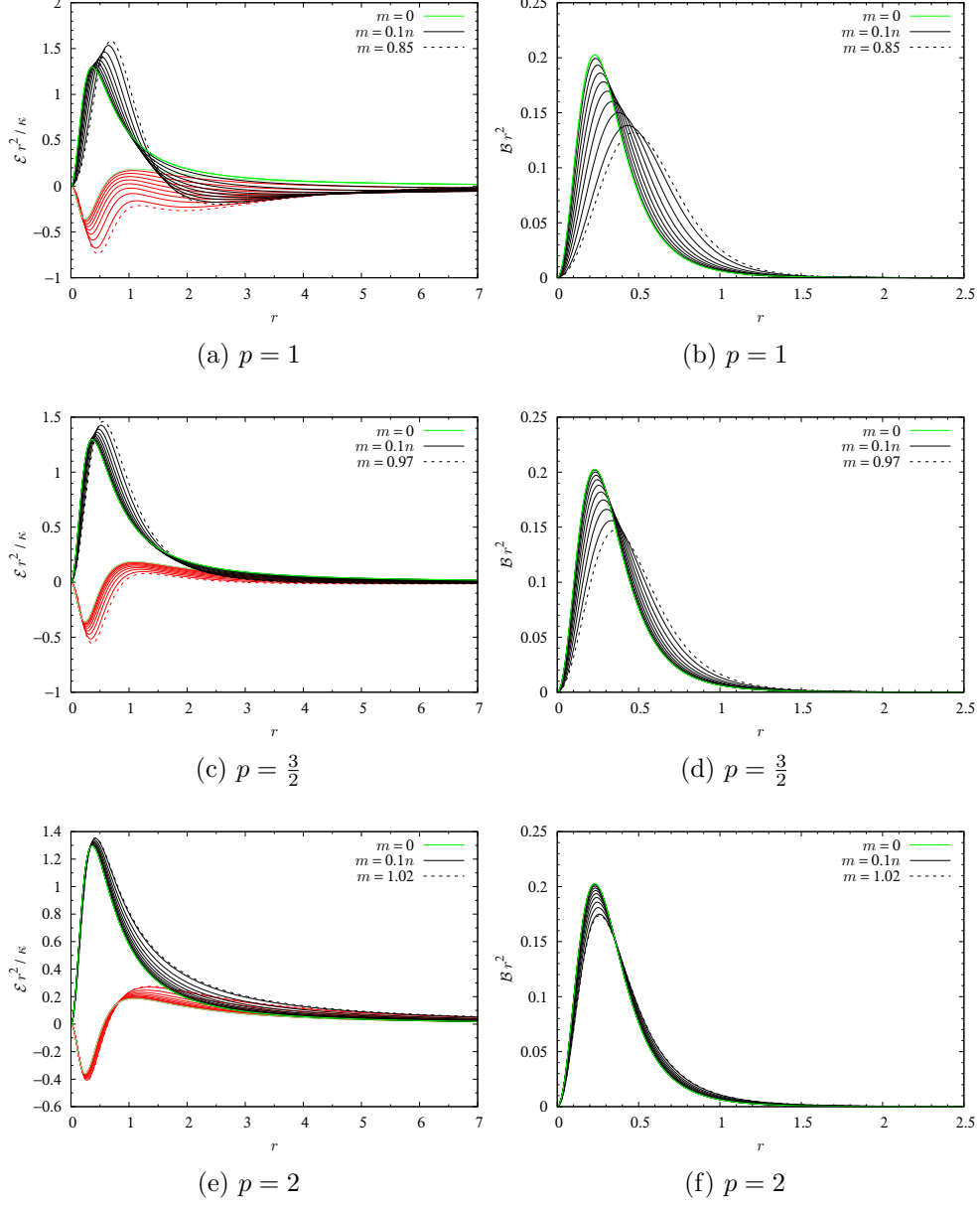


Figure 4: Energy density and topological charge density for magnetic sphalerons with higher-dimensional SO(3)-invariant DM term. Left panels (a,c,e) show the total energy densities weighted with r^2 as black lines and the DM contribution as red lines. Right panels (b,d,f) show the topological charge density, weighted with r^2 . The $m = 0$ solution is shown with a green line (light-green for the DM term) and the m_{crit} solution is shown with a dashed line. The rows of panels correspond to the potential power parameter $p = 1, \frac{3}{2}, 2$.

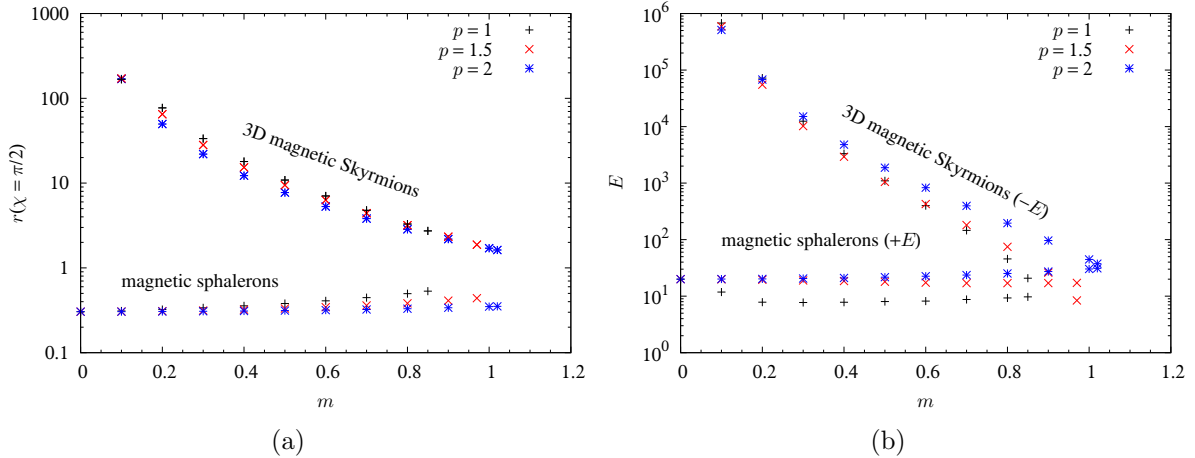


Figure 5: (a) Sizes and (b) energies of magnetic sphalerons (bottom series) versus 3D magnetic Skyrmions (top series) with higher-dimensional $\text{SO}(3)$ -invariant DM term. (a) The size is measured simply by the radius where $\chi = \frac{\pi}{2}$. (b) $-E$ is shown for the magnetic Skyrmions, as they have negative energy (i.e. they are stable solitons). Black pluses correspond to $p = 1$, red crosses to $p = \frac{3}{2}$ and blue plus-crosses to $p = 2$. The critical masses, m_{crit} , correspond to the largest sphalerons and the smallest Skyrmions.

and $-E$ is shown for the magnetic Skyrmion (since it is a logarithmic plot). Clearly, the sphaleron has a larger energy than the magnetic Skyrmion, since it always has the opposite sign than the latter.

Finally, in Fig. 6 we show the energy functional $E(R)$ of Eq. (2.67) for the two cases of $m = 0.3$ and $m = 0.7$ with the potential $p = 1$. It is observed from the figure that the magnetic sphaleron has a positive energy, whereas the magnetic Skyrmion always has a negative energy. Moreover, the scaling of the radii is consistent with Fig. 5; that is, the magnetic sphaleron grows while the magnetic Skyrmion shrinks with increasing m , consistent with Eqs. (2.72) and (2.73).

2.4 A connection to the Hopfion

At present, the 3-dimensional chiral magnetic Skyrmion we proposed stands as a purely theoretical model with no experimental realization, since we require a 4-dimensional magnetization vector. However, our higher-dimensional model can be connected to the model of Hopfions in chiral magnets which have been studied theoretically in Refs. [42, 44, 45] and found experimentally [46, 47]. Magnetic Hopfions have also been studied in frustrated magnets in Ref. [41, 43]. In order to interpolate to the Hopfion model, we need to turn on

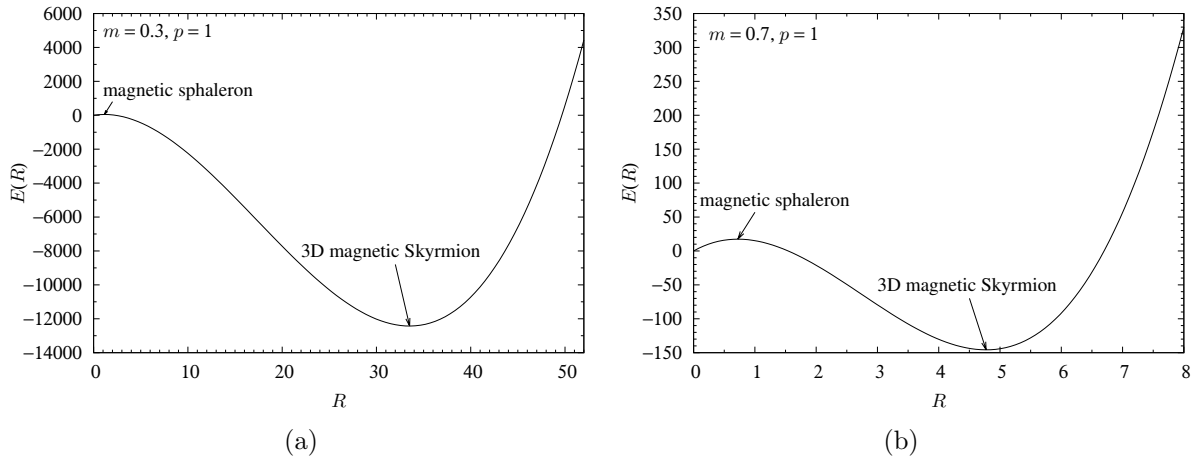


Figure 6: The energy functional $E(R)$ as function of the radius R , illustrating the unstable magnetic sphaleron fixed point at a small radius and the stable magnetic Skyrmion fixed point at a larger radius, for (a) $m = 0.3$ and (b) $m = 0.7$ both with the $p = 1$ potential. It is also observed that the magnetic sphaleron grows with m whereas the magnetic Skyrmion shrinks with m .

an additional deformation potential

$$E_0^{\text{def}}[\mathbf{n}] = \int d^3x m'^2 (n^3)^2, \quad (2.74)$$

so that the theory is $E[\mathbf{n}] + E_0^{\text{def}}[\mathbf{n}]$, with $E[\mathbf{n}]$ of Eq. (2.1). This potential is compatible with the vacuum $\mathbf{N} = (0, 0, 0, 1)^T$, but squeezes the unbroken 2-sphere. In the limit $m' \rightarrow 0$ we return to our higher-dimensional model, whereas in the limit $m' \rightarrow \infty$, the target space is effectively reduced from the 3-dimensional S^3 to the 2-dimensional S^2 . Being too energetically expensive to deviate from $n^3 = 0$, the theory with the SO(3)-invariant higher-dimensional DM term (2.18) reduces in the $m' \rightarrow \infty$ limit to

$$E^{\text{red}}[\mathbf{u}] = \int d^3x \left[\frac{1}{2} \partial_i \mathbf{u} \cdot \partial_i \mathbf{u} + \kappa \alpha \mathbf{u} \cdot \nabla \times \mathbf{u} - \kappa (\beta - \alpha) \epsilon^{ij} u^i \partial_3 u^j - m^2 (1 - u^3) \right], \quad (2.75)$$

where $\mathbf{u} = (-n^2, n^1, n^4) \in S^2$ is the reduced magnetization vector ($\mathbf{u} \cdot \mathbf{u} = 1$). Notice the rotation of the first two magnetization coordinates. Note also that the ∂_3 derivative part of the DM term is proportional to β only. Setting $\beta = \alpha = 1$ simplifies the energy to

$$E^{\text{red}}[\mathbf{u}] = \int d^3x \left[\frac{1}{2} \partial_i \mathbf{u} \cdot \partial_i \mathbf{u} + \kappa \mathbf{u} \cdot \nabla \times \mathbf{u} - m^2 (1 - u^3) \right], \quad (2.76)$$

which is exactly the energy of the Hopfion studied in Refs. [42, 44, 45].

Given that the Derrick's scaling of this theory is identical to our higher-dimensional model with $\mathbf{n} \in S^3$ instead of $\mathbf{u} \in S^2$, we expect that also the magnetic Hopfion model in chiral magnets could have a *sphaleron*, see Sec. 2.3.

A problem with the deformation (2.74) is that the hybrid Skyrmion sector (with S^3 target space) and the Hopfion sector (with S^2 target space) are not connected continuously. Sending $m' \rightarrow \infty$ the Skyrmion mass in the nontrivial sector $\pi_3(S^3)$ goes to infinity. The Hopfion sector, $\pi_3(S^2)$, instead appears at a certain m' as a metastable sector and becomes absolutely stable as $m' \rightarrow \infty$.

3 A magnetic-QCD hybrid Skyrme model

We will now briefly consider the hybrid model consisting of the higher-dimensional magnetic Skyrmion model of Sec. 2 and the standard Skyrme model that is often used in a high-energy context [10, 11]. We do this by amending the energy (2.1) with the so-called Skyrme term, $E_4 = \int d^3\mathcal{E}_4$, whose density is [10, 11]

$$\mathcal{E}_4(\mathbf{n}) = \frac{1}{4e^2} [(\partial_i \mathbf{n} \cdot \partial_i \mathbf{n})(\partial_j \mathbf{n} \cdot \partial_j \mathbf{n}) - (\partial_i \mathbf{n} \cdot \partial_j \mathbf{n})(\partial_i \mathbf{n} \cdot \partial_j \mathbf{n})]. \quad (3.1)$$

This introduces an extra coupling constant or theory parameter, viz. e – not to be confused with the electron charge.

Inserting the hedgehog Ansatz (2.38), the total energy for the magnetic-QCD hybrid Skyrme model reads

$$E = 4\pi \int \left[\frac{1}{2} r^2 (\chi')^2 + \sin^2 \chi + \kappa (r^2 \chi' + r \sin 2\chi) + m^2 r^2 (1 - \cos \chi)^p + \frac{\sin^2 \chi}{e^2} \left((\chi')^2 + \frac{\sin^2 \chi}{2r^2} \right) \right] dr, \quad (3.2)$$

which leads to the equation of motion

$$\chi'' + \frac{2}{r} \chi' - \frac{\sin 2\chi}{r^2} + \frac{4\kappa \sin^2 \chi}{r} - pm^2 (1 - \cos \chi)^{p-1} \sin \chi + \frac{2 \sin^2(\chi) \chi''}{e^2 r^2} + \frac{\sin(2\chi)(\chi')^2}{e^2 r^2} - \frac{\sin^2 \chi \sin 2\chi}{e^2 r^4} = 0. \quad (3.3)$$

The DM term must be negative to stabilize the soliton according to Derrick's theorem. If we add a boundary term $2\pi\kappa\partial_r(r^2 \sin 2\chi)$ to the energy functional, the DM term becomes

negative definite for a monotonically decreasing profile function:

$$E = 4\pi \int \left[\frac{1}{2}r^2(\chi')^2 + \sin^2 \chi + \kappa r^2 \sin^2(\chi)\chi' + m^2 r^2(1 - \cos \chi)^p + \frac{\sin^2 \chi}{e^2} \left((\chi')^2 + \frac{\sin^2 \chi}{2r^2} \right) \right] dr, \quad (3.4)$$

that is, for $\chi(r)$ going monotonically from $\chi(0) = \pi$ to $\chi(\infty) = 0$. We should note that the boundary term only vanishes for exponentially localized solitons ($m \neq 0$), otherwise for massless Skyrmions this boundary term will give a finite, but constant contribution to the energy.

We are now ready to perform a Derrick's scaling analysis next.

3.1 Derrick phase diagram

In this section, we investigate the phase diagram of the theory through Derrick's theorem. Rescaling the lengths as $r \rightarrow \lambda r$, we obtain similarly to the case of the model without the Skyrme term, a scaled energy

$$E_\lambda = \lambda E_2 + \lambda^2 E_1 + \lambda^3 E_0 + \frac{1}{\lambda} E_4. \quad (3.5)$$

Each energy contribution is here approximated to be a constant c_n times the coupling constant times the soliton size R to the power given by the Derrick scaling:

$$\lambda E_2 = c_2 R, \quad \lambda^2 E_1 = -c_1 \kappa R^2, \quad \lambda^3 E_0 = c_0 m^2 R^3, \quad \frac{1}{\lambda} E_4 = \frac{c_4}{e^2 R}. \quad (3.6)$$

This approximate energy functional as a function of the soliton size, R , thus reads

$$E(R) = c_2 R - \kappa c_1 R^2 + m^2 c_0 R^3 + \frac{c_4}{e^2 R}. \quad (3.7)$$

At this point, it will prove useful to choose a particular unit of energy and of length, so as to reduce the variables of the theory. In particular, we have

$$E(\tilde{R}) = \frac{c_2^{\frac{3}{2}}}{\sqrt{c_0} m} \left[\tilde{R} - \tilde{\kappa} \tilde{R}^2 + \tilde{R}^3 + \frac{1}{\tilde{e}^2 \tilde{R}} \right], \quad (3.8)$$

where we have defined

$$\tilde{\kappa} = \frac{\kappa c_1}{\sqrt{c_0 c_2} m}, \quad \tilde{e} = \frac{e c_2}{\sqrt{c_0 c_4} m}, \quad (3.9)$$

and \tilde{R} is given in Eq. (2.68)

Derrick stability is given by imposing the derivative of the above energy with respect to R equal to zero:

$$E'(\tilde{R}) = \frac{c_2^{\frac{3}{2}}}{\sqrt{c_0 m}} \left[1 - 2\tilde{\kappa}\tilde{R} + 3\tilde{R}^2 - \frac{1}{\tilde{e}^2\tilde{R}^2} \right] = 0. \quad (3.10)$$

This is a polynomial equation in \tilde{R} of fourth order,

$$y(\tilde{R}) = \tilde{R}^4 - \frac{2\tilde{\kappa}}{3}\tilde{R}^3 + \frac{1}{3}\tilde{R}^2 - \frac{1}{3\tilde{e}^2} = 0, \quad (3.11)$$

which thus has in principle four roots. Physically, only real and positive roots are relevant though. Deriving this polynomial function with respect to \tilde{R} gives the saddle points:

$$4\tilde{R}^2 - 2\tilde{\kappa}\tilde{R} + \frac{2}{3} = 0, \quad \Rightarrow \quad \tilde{R}_{\pm}^{\text{saddle}} = \frac{1}{4} \left(\tilde{\kappa} \pm \sqrt{\tilde{\kappa}^2 - \frac{8}{3}} \right), \quad (3.12)$$

as well as $\tilde{R} = 0$. There are now four possibilities, if the argument of the square root is positive, there are two saddle points, $\tilde{R}_{\pm}^{\text{saddle}}$ in addition to that at $\tilde{R} = 0$. We assume that $1/\tilde{e} > 0$, i.e. that the Skyrme term is turned on (if not, the analysis of Sec. 2.3 applies). If $y(\tilde{R}_{-}^{\text{saddle}})$ and $y(\tilde{R}_{+}^{\text{saddle}})$ have the same sign, then there is only a single solution. If $y(\tilde{R}_{-}^{\text{saddle}}) > 0$ and $y(\tilde{R}_{+}^{\text{saddle}}) < 0$, there will be three different solutions. The third possibility is that $y(\tilde{R}_{-}^{\text{saddle}}) = 0$ in which case there will be exactly two solutions. The fourth possibility that $y(\tilde{R}_{+}^{\text{saddle}}) = 0$ also yields two solutions. Finally, for $\tilde{\kappa} < \sqrt{8/3}$ the saddle points are not real and there is again only a single solution. There is also only one solution for $\tilde{\kappa} = \sqrt{8/3}$, since $\tilde{R}_{-}^{\text{saddle}}$ coalesces with $\tilde{R} = 0$ and the polynomial will only cross $y = 0$ once, even if that happens at the saddle point $\tilde{R}_{+}^{\text{saddle}}$.

Evaluating the polynomial y at the saddle points gives

$$y(\tilde{R}_{\pm}^{\text{saddle}}) = -\frac{1}{36} - \frac{1}{3\tilde{e}^2} + \frac{1}{864} \left(36\tilde{\kappa}^2 - 9\tilde{\kappa}^4 \pm 8\tilde{\kappa}\sqrt{9\tilde{\kappa}^2 - 24} \mp 3\tilde{\kappa}^3\sqrt{9\tilde{\kappa}^2 - 24} \right). \quad (3.13)$$

We notice, that if $\frac{1}{\tilde{e}^2}$ is too large, both saddle points are negative and only one solution exists. Setting $\tilde{\kappa} = \sqrt{8/3}$, the two saddle point coalesce. In this case, the condition $y(\tilde{R}_{-}^{\text{saddle}}) > 0$ becomes

$$\frac{1}{\tilde{e}^2} \leq \frac{1}{36}, \quad (3.14)$$

with equality at the triple point of the phase diagram. On the other hand, the largest power of $\tilde{\kappa}$ in $y(\tilde{R}_{+}^{\text{saddle}})$ has a negative coefficient, so $y(\tilde{R}_{+}^{\text{saddle}}) < 0$ is always satisfied for large $\tilde{\kappa}$. The condition $y(\tilde{R}_{-}^{\text{saddle}}) \geq 0$ for large $\tilde{\kappa}$ can be simplified by Taylor expansion to

$$\frac{1}{\tilde{e}^2} \leq \frac{1}{27\tilde{\kappa}^2} + \mathcal{O}(\tilde{\kappa}^{-4}). \quad (3.15)$$

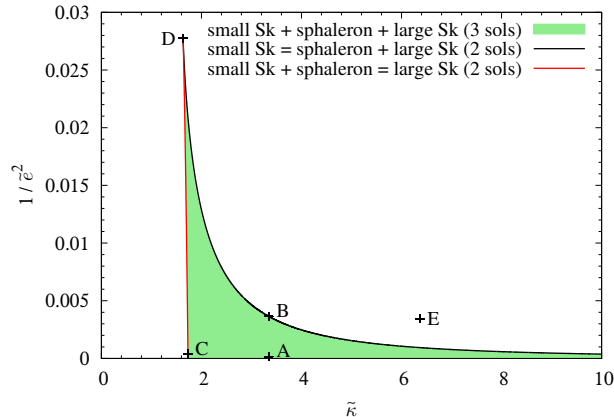


Figure 7: The green shaded area of the phase diagram contains 3 solutions (a small Skyrmion, a sphaleron and a large Skyrmion), the black line corresponds to $y(\tilde{R}_-^{\text{saddle}}) = 0$ for which the small Skyrmion and the sphaleron coalesce, and the red line corresponds to $y(\tilde{R}_+^{\text{saddle}}) = 0$ for which the sphaleron and the large Skyrmion coalesce. In addition there is only 1 solution in the entire white area of the phase diagram. ‘Sk’ in the legend is an abbreviation for Skyrmion.

The possibility for 3 solutions, corresponding to a small Skyrmion, a big Skyrmion and a sphaleron, only exists in a narrow green shaded band shown in Fig. 7. The black line in the figure corresponds to $y(\tilde{R}_-^{\text{saddle}}) = 0$, for which there are two solutions: the small Skyrmion and the sphaleron merge. The red line corresponds to $y(\tilde{R}_+^{\text{saddle}}) = 0$, for which there are also two solutions: the sphaleron and the large Skyrmion merge. It is difficult to see with the naked eye, but the red line is not vertical, but slightly tilted, i.e. it has a large negative derivative with respect to $\tilde{\kappa}$. The triple point of the phase diagram where the black line and the red line meet is at $(\tilde{\kappa}, \tilde{e}^{-2}) = (\sqrt{8/3}, 1/36)$, for which there is only one solution. In the remaining white area of the phase diagram there is only a single solution.

3.2 Numerical magnetic-QCD hybrid Skyrmion solutions

We will now turn to numerical solutions of the equation of motion (3.3) for the magnetic-QCD hybrid Skyrme model. Considering mainly the aspect of the different points in the phase diagram having a different number of solutions, we select 5 characteristic points in the phase diagram labeled as A through E, see Fig. 7.

For the stable and metastable solutions, we use the gradient flow method for finding the numerical solutions. This method is, however, not very effective at finding the unstable solutions, for which we use the shooting method. Knowing the size from the fixed points of the energy (2.67) makes it relatively easy to guess the shooting parameter c , where $\chi = \pi - cr + \mathcal{O}(r^2)$.

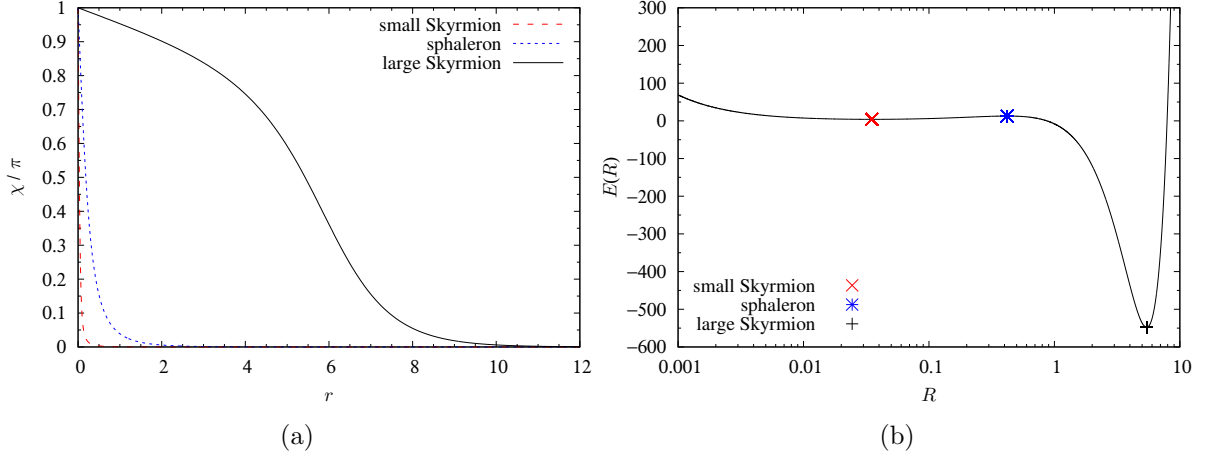


Figure 8: (a) Three different solutions in the magnetic-QCD hybrid Skyrme model at the point in parameter space corresponding to A in the phase diagram 7: the small Skyrmion, the sphaleron and the large Skyrmion; which are metastable, unstable and stable, respectively, as can be seen in panel (b). (b) The energy as function of R , see Eq. (2.67). In this figure $\kappa = 2$ and $1/e^2 = 0.001$ corresponding to $\tilde{\kappa} = 3.34854$ and $1/\tilde{e}^2 = 0.000163315$.

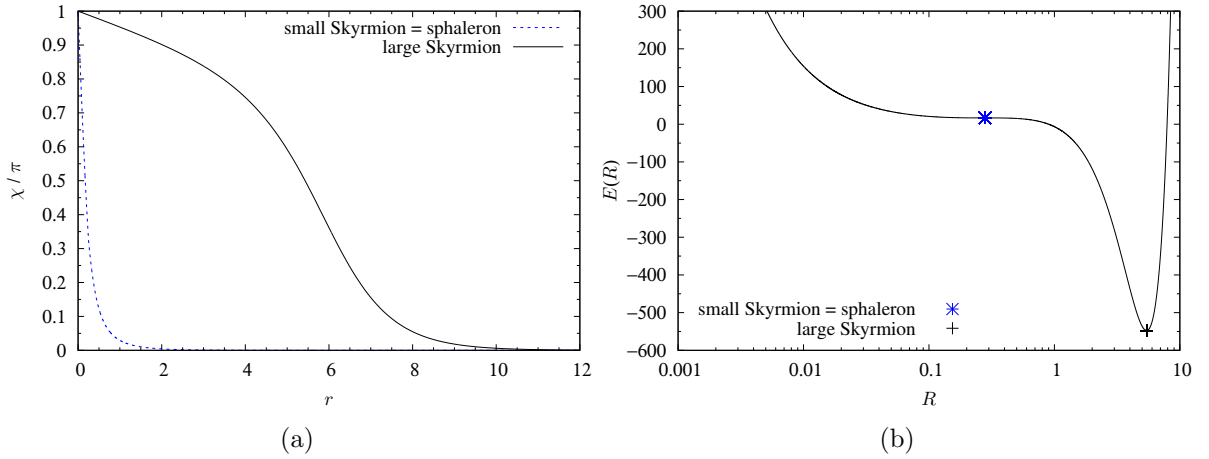


Figure 9: (a) Two different solutions in the magnetic-QCD hybrid Skyrme model at the point in parameter space corresponding to B in the phase diagram 7: the sphaleron and the large Skyrmion; which are unstable and stable, respectively, as can be seen in panel (b). The small Skyrmion and the sphaleron have merged, as this point of the parameter space is on the black line of Fig. 7. (b) The energy as function of R , see Eq. (2.67). In this figure $\kappa = 2$ and $1/e^2 = 0.0222714$ corresponding to $\tilde{\kappa} = 3.34885$ and $1/\tilde{e}^2 = 0.00363763$.

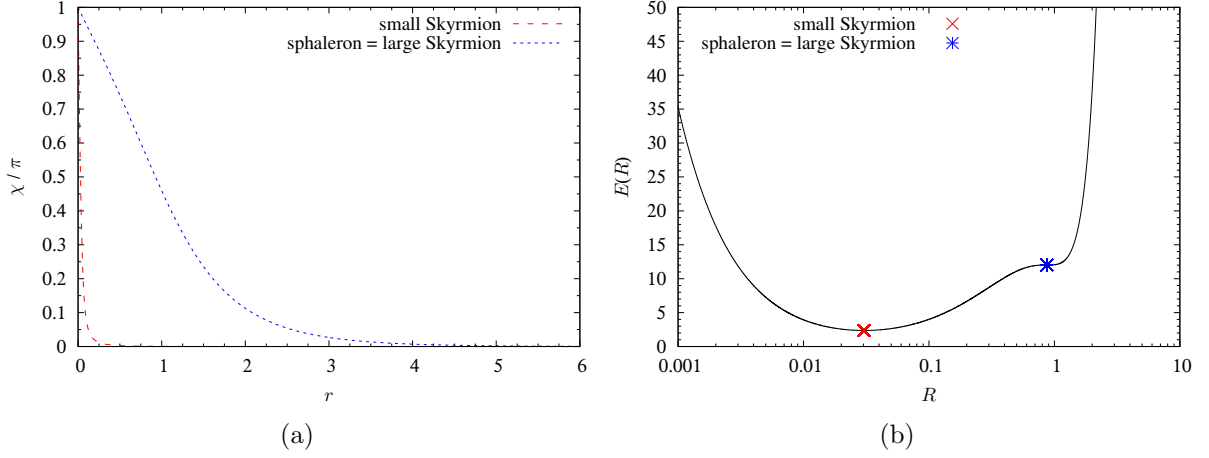


Figure 10: (a) Two different solutions in the magnetic-QCD hybrid Skyrme model at the point in parameter space corresponding to C in the phase diagram 7: the small Skyrmion and the sphaleron; which are stable and unstable, respectively, as can be seen in panel (b). The sphaleron and the large Skyrmion have merged, as this point of the parameter space is on the red line of Fig. 7. (b) The energy as function of R , see Eq. (2.67). In this figure $\kappa = 0.974622$ and $1/e^2 = 0.001$ corresponding to $\tilde{\kappa} = 1.73108$ and $1/\tilde{e}^2 = 0.000375625$.

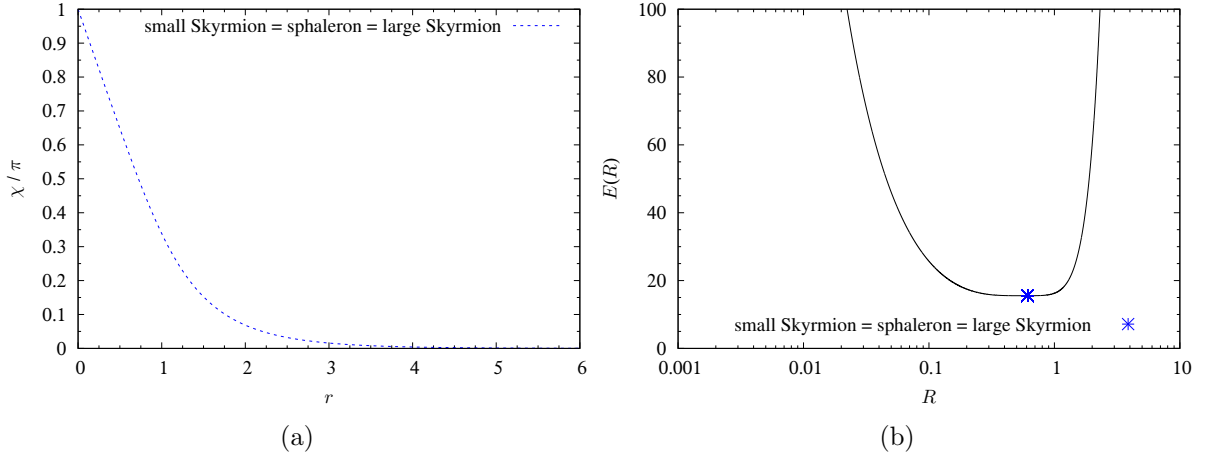


Figure 11: (a) The solution in the magnetic-QCD hybrid Skyrme model at the triple point in parameter space corresponding to D in the phase diagram 7. The small Skyrmion, the sphaleron and the large Skyrmion all have merged at this triple point. (b) The energy as function of R , see Eq. (2.67). In this figure $\kappa = 0.948102$ and $1/e^2 = 0.0654157$ corresponding to $\tilde{\kappa} = \sqrt{8/3}$ and $1/\tilde{e}^2 = 1/36$.

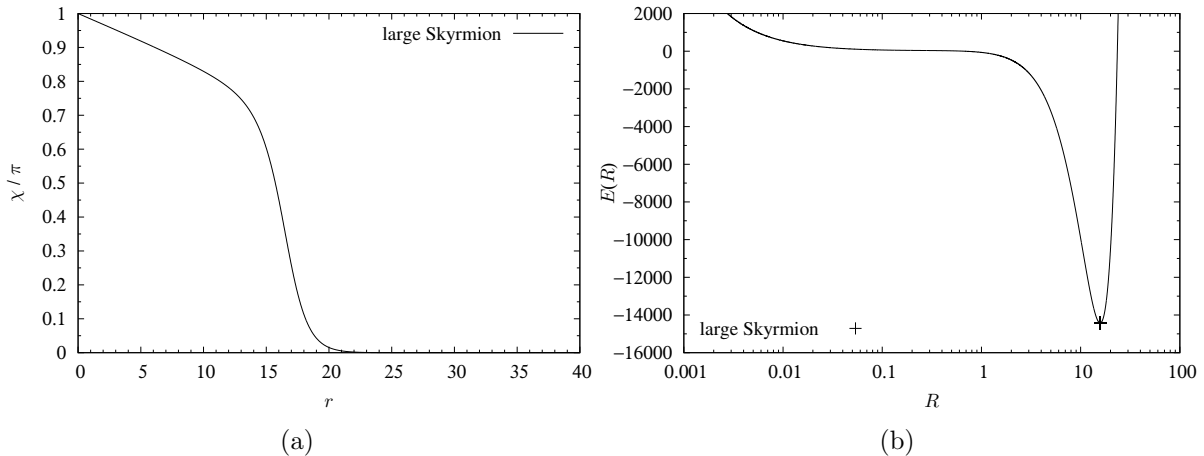


Figure 12: (a) The solution in the magnetic-QCD hybrid Skyrme model at the point in parameter space corresponding to E in the phase diagram 7: the large Skyrmion, which is stable. (b) The energy as function of R , see Eq. (2.67). In this figure $\kappa = 5$ and $1/e^2 = 1/25$ corresponding to $\tilde{\kappa} = 6.37029$ and $1/\tilde{e}^2 = 0.00343907$.

As we can see from the phase diagram in Fig. 7, there are generally 5 different situations: in the green area there are 3 different solutions, on the black and red line there are two different solutions, whereas at the triple point and in the white region, there is only a single solution. For simplicity, we show only one example of each of the 5 different cases.

Starting with the point A of the phase diagram 7, we illustrate the 3 different solutions in Fig. 8 which correspond to the (metastable) small Skyrmion, the (unstable) sphaleron and the (stable) large Skyrmion. At point B of the phase diagram 7, we show two different solutions in Fig. 9 which correspond to the sphaleron and the large Skyrmion; the small Skyrmion and the sphaleron have merged into a single solution, as is shown with a black line in the phase diagram 7. At point C of Fig. 7, we show two different solutions in Fig. 10 corresponding to the small Skyrmion and the sphaleron; in this case the sphaleron and the large Skyrmion have merged, leaving the small Skyrmion as the stable solution. At point D of the phase diagram 7, we show the only existing solution in Fig. 11; this solution is at the triple point of the phase diagram, indicating that all three solutions have merged into a single stable Skyrmion. At point E of Fig. 7, we show the only existing solution in Fig. 12, which is a large Skyrmion and is stable.

3.3 Connecting to the Hopfion

Analogously to the case without the Skyrme term (Sec. 2.4), the hybrid magnetic-QCD Skyrme model can also be connected to Hopfions, which due to the Skyrme term will be

DMI-deformed Faddeev-Skyrme Hopfions. When $\kappa := 0$ it is exactly the Faddeev-Skyrme model [53]. The Derrick scaling of this theory (DMI-deformed Faddeev-Skyrme model) is exactly the same as our hybrid magnetic-QCD Skyrme model. We hence expect that the Hopfion model also contains both a *sphaleron* as well as a small Hopfion, in some parts of the parameter space, similarly to what happened for the Skyrmions in Sec. 3.1.

4 Physical realization of higher-dimensional magnetic solitons

In the realm of quantum simulations for condensed matter phenomena, the idea of “synthetic dimensions” [31, 39] has recently become a valuable tool for replicating effects like topological phases of matter [36, 40], which arise in higher-dimensional physical systems. This concept revolves around connecting certain degrees of freedom, such as various internal states of atoms [33, 34, 38] or photons [35], to emulate the movement of a particle along an additional spatial dimension. Lattice Hamiltonians allow for the simulation of higher-dimensional topological models in lower-dimensional systems, though they require reinterpretation of internal degrees of freedom to emulate an extra spatial dimension. Traditional methods, like embedding higher-dimensional lattices or using topological pumps, are challenging or limited in capturing full dynamics.

In contrast, synthetic dimensions offer an innovative path for lower-dimensional systems to explore higher-dimensional physics. The key idea is to take a set of unconnected internal states within a system and re-imagine them as lattice sites along a spatial dimension. By introducing specific external couplings, particles can effectively “hop” along this synthetic dimension, mimicking movement across a real lattice [32] as shown pictorially in Fig. 13.

What remains to be specified is the nature of the internal states of the system which will effectively act as an extra spatial dimension. For magnetic Hopfions or Skyrmions, the spin-orbit coupling (SOC) is especially promising because it influences chirality and texture stability, giving rise to complex configurations that could correspond to synthetic 4D behavior. We leave the search for the exact physical system that could be a candidate for providing the synthetic dimension for our higher-dimensional version of the DM interaction for future work.

In Fig. 14 we illustrate an example of a Skyrmion when the n^3 element of the 4-dimensional magnetization vector correspond to the synthetic dimension.

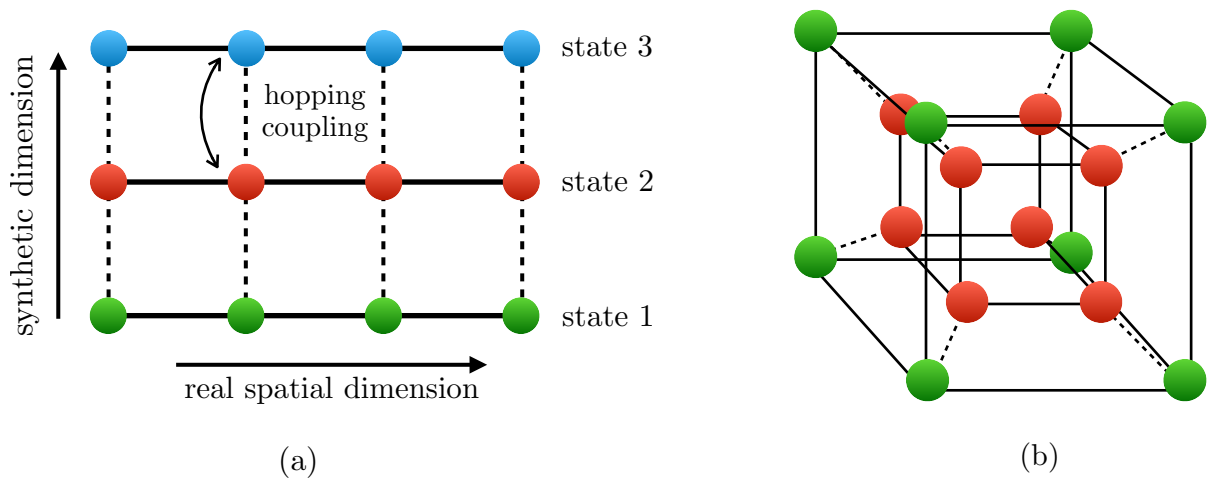


Figure 13: Synthetic dimensions transform internal states or intrinsic properties into an effective spatial dimension. (a) A 2D discrete lattice model includes one real spatial dimension and one synthetic dimension composed of spin states. Hopping along the real dimension (solid lines) represents actual particle motion, while hopping along the synthetic dimension (dashed lines) corresponds to externally induced transitions between spin states. (b) A 4D hypercubic lattice illustrates a combination of real and synthetic spatial dimensions, showcasing how higher-dimensional structures can emerge in lower-dimensional systems.

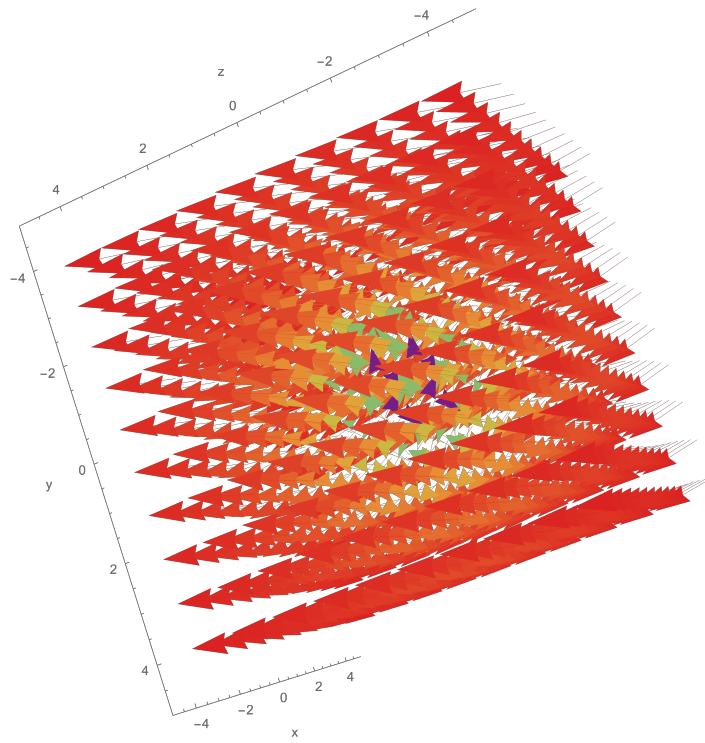


Figure 14: Illustration of the magnetization vector in an example where the physical dimensions are mapped as $\mathbf{n} = (n^x, n^y, n^{\text{synth}}, n^z)$, with n^{synth} representing the component of the would-be magnetization vector in the synthetic dimension.

5 Conclusion

In this paper, we have generalized the Dzyaloshinskii-Moriya interaction for a 3D magnetization vector to a 4D magnetization vector – hence a higher-dimensional version of the DMI. Using the property that it is first order in derivatives and must be nonvanishing, we deduced that it must be contracted with a tensor that is antisymmetric in $O(4)$ -indices and bears a 3D spatial index. Considering furthermore the simplified case of $SO(3)$ invariance, we are able to reduce the DM term to just two invariant structures, that we denote the α and β parts. It turns out that the β -part is irrelevant for the spherically symmetric case and only the α -part stabilizes the solitons. Due to the higher dimension of space, there are in fact two solitons with just the DMI and a potential: the Skyrmion and a sphaleron, where the latter is an unstable and smaller solution of the model. Upon reduction to the Hopfion model, the β -part nevertheless plays an important role. Finally, we consider including the Skyrme term, thus considering a magnetic-QCD hybrid Skyrme model that turns out to host a large and a small Skyrmion as well as a sphaleron – at least in a small region of parameter space of the model. The large Skyrmion is stable, the small Skyrmion is metastable and the sphaleron is unstable. The phase diagram is quite rich and there exist lines where the different types of solutions coalesce and in the remaining part of the parameter space of the model, there exists only one solution – the Skyrmion.

We have contemplated that by using a synthetic extra dimension, it would be possible to construct our higher-dimensional magnetic Skyrmion or perhaps the hybrid Skyrmion in a physically realizable condensed matter system. The details of whether the exact Hamiltonian corresponding to our model can be constructed, still needs to be worked out.

We have focused on spherically symmetric solitons in this paper. Using the spherically symmetric hedgehog Ansatz, we found that β -part of the $SO(3)$ -invariant DM term (2.18) vanishes and so we effectively only used the α -part of the $SO(3)$ -invariant DM term. Deformed solitons, however, may feel the presence of the β -part of the DM term, which in principle could lower the mass of the soliton. We leave the exploration of such a possibility for future work.

We also considered a connection to the Hopfion in chiral magnets, and although there exists a higher-dimensional DM term and a potential with a limit that connects to the Hopfion model, the interpolation is not expected to be smooth. That is, the topology changes, sending the masses of the nontrivial $\pi_3(S^3)$ solitons to infinity and the nontrivial $\pi_3(S^2)$ solitons appear first as metastable and then finally become stable at the end point of the limit. A smooth interpolation is thus desirable and will be left for future work.

In summary, this work presents an initial study of a generalized model for higher-dimensional magnetic Skyrmions, revealing rich solitonic physics.

Acknowledgments

S. B. G. thanks the Outstanding Talent Program of Henan University and the Ministry of Education of Henan Province for partial support. The work of S. B. G. is supported by the National Natural Science Foundation of China (Grant No. 12071111) and by the Ministry of Science and Technology of China (Grant No. G2022026021L). The work of S. B. is supported by the INFN special research project grant “GAST” (Gauge and String Theories).

References

- [1] A. N. Bogdanov and D. A. Yablonskii, *Thermodynamically stable “vortices” in magnetically ordered crystals. The mixed state of magnets*, *Soviet Journal of Experimental and Theoretical Physics* **68** (Jan., 1989) 101.
- [2] A. Bogdanov, *New localized solutions of the nonlinear field equations*, *Soviet Journal of Experimental and Theoretical Physics Letters* **62** (Aug., 1995) 247.
- [3] N. Nagaosa and Y. Tokura, *Topological properties and dynamics of magnetic skyrmions*, *Nat. Nanotechnol.* **8** (2013) 899.
- [4] S. Mühlbauer, B. Binz, F. Jonietz, C. Pfleiderer, A. Rosch, A. Neubauer, R. Georgii, and P. Böni, *Skyrmion lattice in a chiral magnet*, *Science* **323** (2009), no. 5916 915–919.
- [5] X. Z. Yu, Y. Onose, N. Kanazawa, J. H. Park, J. H. Han, Y. Matsui, N. Nagaosa, and Y. Tokura, *Real-space observation of a two-dimensional skyrmion crystal*, *Nature* **465** (Jun, 2010) 901–904.
- [6] A. Fert, N. Reyren, and V. Cros, *Magnetic skyrmions: advances in physics and potential applications*, *Nature Reviews Materials* **2** (Jun, 2017) 17031.
- [7] K. Everschor-Sitte, J. Masell, R. M. Reeve, and M. Kläui, *Perspective: Magnetic skyrmions—Overview of recent progress in an active research field*, *Journal of Applied Physics* **124** (12, 2018) 240901.
- [8] S. Luo and L. You, *Skyrmion devices for memory and logic applications*, *APL Materials* **9** (05, 2021) 050901.
- [9] C. Psaroudaki, E. Peraticos, and C. Panagopoulos, *Skyrmion qubits: Challenges for future quantum computing applications*, *Applied Physics Letters* **123** (12, 2023) 260501.

- [10] T. H. R. Skyrme, *A non-linear field theory*, *Proceedings of the Royal Society of London. Series A. Mathematical and Physical Sciences* **260** (1961), no. 1300 127–138.
- [11] T. H. R. Skyrme, *A unified field theory of mesons and baryons*, *Nuclear Physics* **31** (1962) 556–569.
- [12] E. Witten, *Global Aspects of Current Algebra*, *Nucl. Phys. B* **223** (1983) 422–432.
- [13] E. Witten, *Current Algebra, Baryons, and Quark Confinement*, *Nucl. Phys. B* **223** (1983) 433–444.
- [14] T. Sakai and S. Sugimoto, *Low energy hadron physics in holographic QCD*, *Prog. Theor. Phys.* **113** (2005) 843–882, [[hep-th/0412141](#)].
- [15] U. K. Röbner, A. N. Bogdanov, and C. Pfeleiderer, *Spontaneous skyrmion ground states in magnetic metals*, *Nature* **442** (Aug, 2006) 797–801.
- [16] U. Rossler, A. A. Leonov, and A. N. Bogdanov, *Chiral Skyrmionic matter in non-centrosymmetric magnets*, *J. Phys. Conf. Ser.* **303** (2011) 012105, [[arXiv:1009.4849](#)].
- [17] M. Ezawa, *Compact Skyrmions, Merons and Bimerons in Thin Chiral Magnetic Films*, *Phys. Rev. B* **83** (2011) 100408, [[arXiv:1010.4119](#)].
- [18] S. Banerjee, J. Rowland, O. Erten, and M. Randeria, *Skyrmions in two-dimensional chiral magnets*, *Phys. Rev. X* **4** (2014), no. 3 031045, [[arXiv:1402.7082](#)].
- [19] C. Melcher, *Chiral skyrmions in the plane*, *Proceedings of the Royal Society A: Mathematical, Physical and Engineering Sciences* **470** (2014), no. 2172 20140394.
- [20] F. N. Rybakov and N. S. Kiselev, *Chiral magnetic skyrmions with arbitrary topological charge*, *Phys. Rev. B* **99** (2019), no. 6 064437, [[arXiv:1806.00782](#)].
- [21] B. J. Schroers, *Gauged Sigma Models and Magnetic Skyrmions*, *SciPost Phys.* **7** (2019), no. 3 030, [[arXiv:1905.06285](#)].
- [22] B. Barton-Singer, C. Ross, and B. J. Schroers, *Magnetic Skyrmions at Critical Coupling*, *Commun. Math. Phys.* **375** (2020), no. 3 2259–2280, [[arXiv:1812.07268](#)].
- [23] V. M. Kuchkin, B. Barton-Singer, F. N. Rybakov, S. Blügel, B. J. Schroers, and N. S. Kiselev, *Magnetic skyrmions, chiral kinks and holomorphic functions*, *Phys. Rev. B* **102** (2020), no. 14 144422, [[arXiv:2007.06260](#)].
- [24] C. Ross, N. Sakai, and M. Nitta, *Skyrmion interactions and lattices in chiral magnets: analytical results*, *JHEP* **02** (2021) 095, [[arXiv:2003.07147](#)].

- [25] D. Hill, V. Slastikov, and O. Tchernyshyov, *Chiral magnetism: a geometric perspective*, *SciPost Phys.* **10** (2021) 078.
- [26] B. Schroers, *Solvable Models of Magnetic Skyrmions*, in *11th International Symposium on Quantum Theory and Symmetries*, 10, 2019. [arXiv:1910.13907](#).
- [27] Y. Amari, Y. Akagi, S. B. Gudnason, M. Nitta, and Y. Shnir, *CP2 skyrmion crystals in an SU(3) magnet with a generalized Dzyaloshinskii-Moriya interaction*, *Phys. Rev. B* **106** (2022), no. 10 L100406, [[arXiv:2204.01476](#)].
- [28] F. Hanada and N. Sawado, *A baby Skyrme model with anisotropic DM interaction: Compact skyrmions revisited*, *Nucl. Phys. B* **996** (2023) 116377, [[arXiv:2303.15751](#)].
- [29] G. H. Derrick, *Comments on nonlinear wave equations as models for elementary particles*, *J. Math. Phys.* **5** (1964) 1252–1254.
- [30] R. Menta, *Magnetic skyrmions and possible extensions*, *ETD (Master Thesis) University of Pisa* (2023).
- [31] O. Boada, A. Celi, J. I. Latorre, and M. Lewenstein, *Quantum simulation of an extra dimension*, *Phys. Rev. Lett.* **108** (Mar, 2012) 133001.
- [32] A. Celi, P. Massignan, J. Ruseckas, N. Goldman, I. B. Spielman, G. Juzeliūnas, and M. Lewenstein, *Synthetic gauge fields in synthetic dimensions*, *Phys. Rev. Lett.* **112** (Jan, 2014) 043001.
- [33] T. Ozawa, H. M. Price, N. Goldman, O. Zilberberg, and I. Carusotto, *Synthetic dimensions in integrated photonics: From optical isolation to four-dimensional quantum Hall physics*, *Phys. Rev. A* **93** (2016), no. 4 043827, [[arXiv:1510.03910](#)].
- [34] H. M. Price, O. Zilberberg, T. Ozawa, I. Carusotto, and N. Goldman, *Four-dimensional quantum hall effect with ultracold atoms*, *Phys. Rev. Lett.* **115** (Nov, 2015) 195303.
- [35] L. Yuan, Q. Lin, M. Xiao, and S. Fan, *Synthetic dimension in photonics*, *Optica* **5** (Nov, 2018) 1396–1405.
- [36] T. Ozawa and H. M. Price, *Topological quantum matter in synthetic dimensions*, *Nature Reviews Physics* **1** (May, 2019) 349–357.
- [37] Y. Wang, H. M. Price, B. Zhang, and Y. D. Chong, *Circuit implementation of a four-dimensional topological insulator*, *Nature Communications* **11** (May, 2020) 2356.

- [38] H. Price, *Simulating four-dimensional physics in the laboratory*, *Physics Today* **75** (04, 2022) 38–44.
- [39] K. R. A. Hazzard and B. Gadway, *Synthetic dimensions*, *Physics Today* **76** (04, 2023) 62–63.
- [40] J. Arguello-Luengo, U. Bhattacharya, A. Celi, R. W. Chhajlany, T. Grass, M. Plodzien, D. Rakshit, T. Salamon, P. Stornati, L. Tarruell, and M. Lewenstein, *Synthetic dimensions for topological and quantum phases*, *Communications Physics* **7** (May, 2024) 143.
- [41] P. Sutcliffe, *Skyrmion knots in frustrated magnets*, *Phys. Rev. Lett.* **118** (2017), no. 24 247203, [[arXiv:1705.10966](https://arxiv.org/abs/1705.10966)].
- [42] P. Sutcliffe, *Hopfions in chiral magnets*, *J. Phys. A* **51** (2018), no. 37 375401, [[arXiv:1806.06458](https://arxiv.org/abs/1806.06458)].
- [43] P. Sutcliffe, *Hopfions*, *Reviews in Mathematical Physics* **30** (2018), no. 08 1840017.
- [44] J.-S. B. Tai and I. I. Smalyukh, *Static Hopf Solitons and Knotted Emergent Fields in Solid-State Noncentrosymmetric Magnetic Nanostructures*, *Phys. Rev. Lett.* **121** (2018), no. 18 187201, [[arXiv:1806.00453](https://arxiv.org/abs/1806.00453)].
- [45] Y. Liu, R. K. Lake, and J. Zang, *Binding a hopfion in a chiral magnet nanodisk*, *Phys. Rev. B* **98** (Nov, 2018) 174437.
- [46] P. J. Ackerman and I. I. Smalyukh, *Static three-dimensional topological solitons in fluid chiral ferromagnets and colloids*, *Nature Materials* **16** (Apr, 2017) 426–432.
- [47] N. Kent, N. Reynolds, D. Raftrey, I. T. G. Campbell, S. Virasawmy, S. Dhuey, R. V. Chopdekar, A. Hierro-Rodriguez, A. Sorrentino, E. Pereiro, S. Ferrer, F. Hellman, P. Sutcliffe, and P. Fischer, *Creation and observation of hopfions in magnetic multilayer systems*, *Nature Communications* **12** (Mar, 2021) 1562.
- [48] I. Dzyaloshinsky, *A thermodynamic theory of “weak” ferromagnetism of antiferromagnetics*, *Journal of Physics and Chemistry of Solids* **4** (1958), no. 4 241–255.
- [49] T. Moriya, *Anisotropic superexchange interaction and weak ferromagnetism*, *Phys. Rev.* **120** (Oct, 1960) 91–98.
- [50] T. Moriya, *New mechanism of anisotropic superexchange interaction*, *Phys. Rev. Lett.* **4** (Mar, 1960) 228–230.

- [51] N. S. Manton, *The Inevitability of Sphalerons in Field Theory*, *Phil. Trans. Roy. Soc. Lond. A* **377** (2019), no. 2161 20180327, [[arXiv:1903.11573](#)].
- [52] S. Bolognesi, S. B. Gudnason, and R. Menta, *Magnetic skyrmions: From lumps to supercompactons*, *Phys. Rev. Res.* **6** (Nov, 2024) 043162, [[arXiv:2406.03941](#)].
- [53] L. D. Faddeev, *Quantization of solitons*, *Princeton preprint IAS-75* (1975) QS70.